HHS Public Access

Author manuscript

Cell Rep. Author manuscript; available in PMC 2026 January 21.

Published in final edited form as:

Cell Rep. 2025 December 23; 44(12): 116643. doi:10.1016/j.celrep.2025.116643.

eIF3d and eIF3e mediate selective translational control of hypoxia that can be inhibited by small molecules

Stephen C. Purdy[1,2], **Kate Matlin**[1,3,4], **Christopher Alderman**[3,4,6], **Amber Baldwin**[3], **Natasha Shrivastava**[1], **Goksu Sarioglu**[1,2], **Somnath Dutta**[8], **Kristofor J. Webb**[7], **Arthur Wolin**[1,4], **Dillon P. Boulton**[1,5], **Annika Gustafson**[1,4,6], **Jyoti Kapali**[9], **John D. Landua**[9], **Michael T. Lewis**[9], **M. Cecilia Caino**[1,2,4,5], **James C. Costello**[1,2,5,6], **William Old**[7,10], **Xiang Wang**[1,8], **Rui Zhao**[2,3,4,6,*], **Heide L. Ford**[1,2,4,5,6,*], **Neelanjan Mukherjee**[3,4,11,*]

[1] Department of Pharmacology, University of Colorado Anschutz Medical Campus (AMC), Aurora, CO, USA

[2] Cancer Biology Program, University of Colorado Anschutz Medical Campus (AMC), Aurora, CO, USA

[3] Department of Biochemistry and Molecular Genetics, University of Colorado Anschutz Medical Campus (AMC), Aurora, CO, USA

[4] Molecular Biology Program, University of Colorado Anschutz Medical Campus (AMC), Aurora, CO, USA

[5] Pharmacology and Molecular Medicine Program, University of Colorado Anschutz Medical Campus (AMC), Aurora, CO, USA

[6] Medical Scientist Training Program, University of Colorado Anschutz Medical Campus (AMC), Aurora, CO, USA

[7] Department of Molecular, Cellular, and Developmental Biology, University of Colorado, Boulder, CO, USA

[8] Department of Chemistry, University of Colorado, Boulder, CO, USA

[9] Departments of Molecular and Cellular Biology and Radiology, Lester and Sue Smith Breast Center, Dan L. Duncan Comprehensive Cancer Center, Baylor College of Medicine, Houston, TX, USA

[10] Present address: Enveda, 5700 Flatiron Parkway, Boulder, CO 80301, USA

*Correspondence: rui.zhao@cuanschutz.edu (R.Z.), heide.ford@cuanschutz.edu (H.L.F.), neelanjan.mukherjee@cuanschutz.edu (N.M.).

AUTHOR CONTRIBUTIONS

Conceptualization, S.C.P., K.M., R.Z., N.M., and H.L.F.; investigation, S.C.P., K.M., C.A., A.B., N.S., S.D., K.J.W., A.W., D.P.B., J.K., J.D.L., G.S., and A.G.; supervision, M.C.C., J.C.C., M.T.L., W.O., X.W., R.Z., N.M., and H.L.F.; writing – original draft, S.C.P. and K.M.; writing – review & editing, S.C.P., K.M., R.Z., N.M., and H.L.F.

DECLARATION OF INTERESTS

A patent application has been filed (X.W., W.O., R.Z., and H.L.F.) on “Small molecules targeting eIF3e to inhibit tumor growth progression, and metastasis,” application no. 18/839,131.

DECLARATION OF GENERATIVE AI AND AI-ASSISTED TECHNOLOGIES IN THE WRITING PROCESS

No generative AI or AI-assisted technologies were used during the preparation of this work.

[11] Lead contact

SUMMARY

Exposure to hypoxia is linked to increased cellular plasticity and enhanced metastasis, effects that are primarily attributed to the transcriptional activation of large gene programs downstream of hypoxia-inducible factors (HIFs). However, translational effects in hypoxia, which likely precede transcriptional effects, have remained largely unexplored. Using ribosome profiling, we uncovered a selective translational response in acute hypoxia that is eukaryotic initiation factor (eIF)3d/eIF3e dependent and controls downstream hypoxic responses, including HIF1α accumulation and cellular invasion. We further demonstrated that eIF3e copy number and eIF3e and eIF3d expression signatures are associated with worsened outcomes for patients with breast cancer. Finally, we identified a class of novel small molecules that target eIF3e specifically, reducing the translational response to hypoxia and to endoplasmic reticulum (ER) stress, another stressor that is dependent on eIF3d-/eIF3e-mediated translation. Our data uncover critical functions for eIF3d/eIF3e in the hypoxic response and identify a potential means to inhibit stress-induced translation, and potentially plasticity and metastasis, mediated by eIF3e.

In brief

Purdy et al. report that eIF3e/eIF3d are required for hypoxia-induced selective mRNA translation and induction of pro-metastatic phenotypes. eIF3e and eIF3d RNA signatures correlate with worsened overall survival in patients with breast cancer, and the acute translational hypoxic response mediated by eIF3e/eIF3d can be inhibited by novel small molecules.

Graphical Abstract

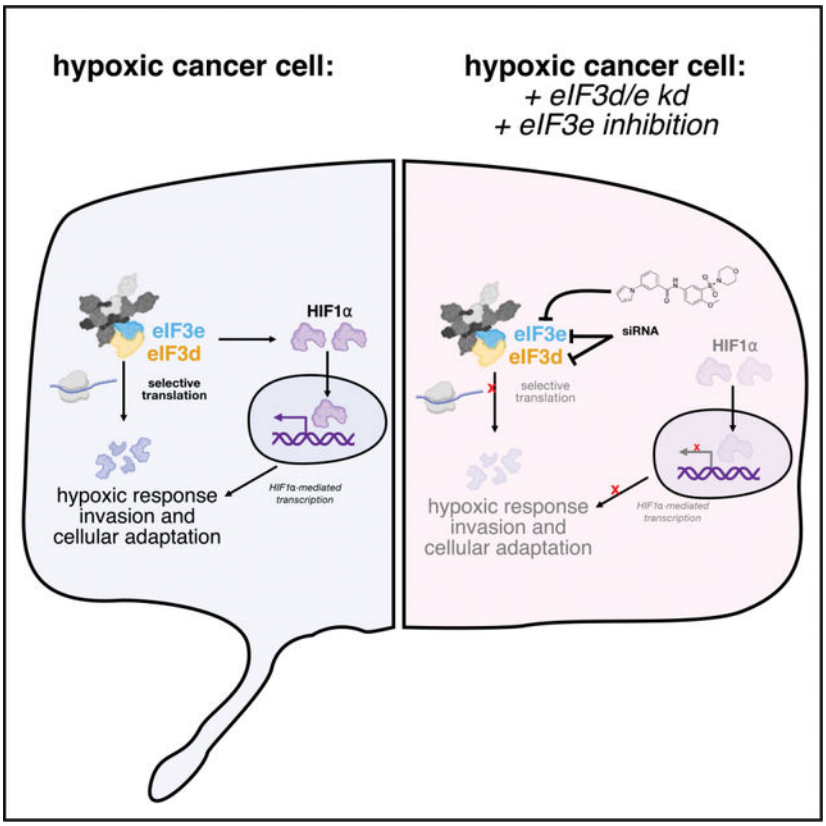

INTRODUCTION

Despite numerous advances in cancer therapies, breast cancer remains the second leading cause of cancer-related deaths among women.[1,2] Importantly, nearly all breast-cancer-related deaths are attributed to metastatic disease,[3] yet a means to target metastasis remains elusive. As cancer cells metastasize, they are exposed to numerous stressors that they must overcome to survive, grow, and metastasize.[4] Recently, the plasticity of mRNA translation has been found to play a critical role in this adaptation.[5,6] Furthermore, translational reprogramming is a major driver of therapeutic resistance leading to poor prognosis.[5,7] Translation dysregulation has long been appreciated in cancer initiation and growth. MAPK and mTOR pathways are often highly activated in tumors and largely contribute to tumor cells' ability to meet the increased protein synthesis demand during oncogenesis.[8–10] Furthermore, alterations in expression of ribosomal proteins and eukaryotic initiation factors (eIFs) are common in cancer, with many eIFs having defined oncogenic roles.[8]

Alterations in the translational response to stress can occur independent of transcriptional alterations, resulting in more immediate phenotypic responses. Thus, rapid translational changes are vital for adaptation to stress.[11,12] Many stressors are experienced by metastatic cells, such as nutrient deprivation and hypoxia, which cause canonical cap-dependent translation to decrease.[13] A reduction in translation allows cells to conserve energy and building blocks (e.g., amino acids) by limiting the high energy demands of protein synthesis.[12] However, while canonical cap-dependent translation is diminished under various

stressors, subsets of mRNAs are selectively translated via non-canonical mechanisms of translation. Selective translation of subsets of mRNAs can be critical for the survival of cells in response to stress and thus may be a major contributor to tumor progression and metastasis. Recently, members of the eIF3 complex have been implicated in selective translation during stress.[14–17]

The eIF3 complex is composed of 13 subunits, providing a large scaffold that is essential for the formation of the 48S preinitiation complex and subsequent translation initiation.[18–21] While the scaffolding function of eIF3 is vital to canonical translation,[21] separable functions have been ascribed to particular subunits of the eIF3 complex that allow for very precise regulation of canonical and non-canonical translation.[14–16,21–32] For example, eIF3d is now known to bind the 5′ m7G cap of specific mRNAs with stem-loop structures in the 5′ UTR.[23] This cap-binding activity allows eIF3d to promote or repress the translation of specific mRNAs.[22,23] Such non-canonical eIF3d-mediated translation is upregulated during cellular stress, specifically during glucose deprivation and chronic endoplasmic reticulum (ER) stress to promote survival. [14,15] Additionally, eIF3d is known to promote the epithelial-to-mesenchymal transition (EMT) and may enhance breast cancer metastasis, though direct evidence that eIF3d mediates metastasis is lacking.[33]

The direct binding partner of eIF3d, eIF3e, has also been implicated in cancer, and like eIF3d, it regulates the translation of a subset of mRNAs in response to various stressors. However, the direct mechanism of eIF3e's selective translational regulation remains unknown.[34] The role of eIF3e in tumor progression is complex; it has been reported to be either tumor suppressive or promotional, dependent on the context.[35–43] Nonetheless, both eIF3d and eIF3e have described tumor promotional roles, and their ability to regulate selective translation may be critical to tumor progression. While several studies have elucidated functions for eIF3d or eIF3e individually under basal conditions, few studies have focused on both proteins simultaneously, particularly during cellular stress, to uncover their overlapping and distinct functions, which would provide important regulatory insights.

One of the most common stressors within the tumor is hypoxia. Hypoxia occurs in 50%–60% of solid tumors and is well known to promote metastasis via multiple mechanisms. [4] A majority of the tumor promotional effects of hypoxia are attributed to the downstream transcriptional regulation by hypoxia-inducible factors (HIFs).[4] Under normoxic conditions, HIF1α and HIF2α are constitutively expressed but rapidly degraded by oxygen-dependent prolyl hydroxylases (PHDs). However, during low-oxygen conditions, PHDs are inhibited, which allows for the rapid accumulation of HIFα proteins. HIFα proteins can then bind to HIF1β (also known as ARNT) and act as pleiotropic transcription factors to regulate the expression of genes involved in angiogenesis, survival, metabolism, and proliferation, among other properties.[44] Thus, transcriptional reprogramming in response to hypoxia has been well documented[45,46]; however, the role of non-canonical translation in response to hypoxia and the factors governing it is largely unexplored.

Herein, we determine the contributions of eIF3d and eIF3e to translational regulation under both normoxic and hypoxic conditions. In normoxia, we identify shared and unique mRNAs that are regulated by eIF3d and eIF3e. We demonstrate that the acute response to hypoxia

is predominately regulated translationally, with few changes in RNA levels. We find that, in most cases, more mRNAs are translationally regulated by eIF3d and eIF3e in hypoxia compared to normoxia and that both subunits of the eIF3 complex are required for hypoxic-induced invasion, demonstrating that their role in selective translation in a reduced oxygen environment mediates phenotypes associated with metastasis. Furthermore, we identify an acute translational hypoxic response that requires eIF3d and eIF3e. We find that eIF3e copy-number gain and both eIF3d and eIF3e RNA signatures strongly correlate with worsened overall survival in breast cancer. Importantly, we identify a class of novel small molecules that target eIF3e, inhibiting the acute hypoxic response as well as hypoxia-induced invasion. We further show that this novel class of inhibitors targets stress-induced translation of ATF4 in response to ER stress, another stress response mediated by eIF3d/eIF3e. Taken together, we demonstrate a critical role for eIF3d and eIF3e in the hypoxic response and identify first-in-class inhibitors of eIF3e. Such compounds will not only serve as important research tools to understand the function of eIF3e in stress-induced translation but may also be starting points for developing novel therapeutic interventions for metastasis.

RESULTS

eIF3e and eIF3d have overlapping and distinct functions

To delineate overlapping and distinct functions of eIF3d and eIF3e (a schematic of the complex is shown in Figure 1A), we performed ribosome profiling (Ribo-seq) in parallel with RNA sequencing (RNA-seq) in a metastatic breast cancer cell line, MCF7-SIX1,[47,48] after small interfering RNA (siRNA)-mediated knockdown (KD) of eIF3e (si3e), eIF3d (si3d), or scramble control (siCtrl). Briefly, Ribo-seq identifies the positions of the ribosome on RNAs by isolating and sequencing the ribosome-protected fragments (RPFs)[49] (Figure 1B). Furthermore, one can calculate the translational efficiency (TE) of an individual RNA by comparing the ratio of RPFs to RNA and determining how these ratios change across conditions to identify mRNAs subject to translational regulation. Biological replicates for both RNA-seq and Ribo-seq were highly reproducible (RNA-seq R = 0.98, Ribo-seq R = 0.96) (Figure S1A). All Ribo-seq datasets exhibited the expected ~29-nt RPF lengths (Figure S1B), enrichment in the coding sequence (Figure S1C), frame preference (Figure S1D), and three-nucleotide periodicity (Figure S1E). We observed the expected reduction in eIF3e and eIF3d protein levels after their respective depletion (Figure 1C). While eIF3e KD reduced eIF3d protein levels, which has been observed in other systems,[50] it did not decrease the mRNA levels or RPFs of eIF3d (Figure S1F). These data suggest that eIF3e does not control eIF3d levels via transcription, mRNA decay, or translation but that it may instead stabilize eIF3d protein post-translationally. Since eIF3d protein levels decrease with eIF3e KD, loss of eIF3d may be responsible for a portion of the mRNA translational changes observed with the KD of eIF3e.

To identify the mRNAs translationally regulated by eIF3d/e, we calculated TE changes upon KD of eIF3d/e compared to the control siRNA.[51] Loss of eIF3d or eIF3e resulted in significantly altered TE of 742 or 521 mRNAs, respectively (Figure 1D). Similar numbers of mRNAs were upregulated (repressed by eIF3d/e) and downregulated (promoted by eIF3d/e) upon eIF3d/e KD. There was a statistically significant overlap of 239 mRNAs regulated

by both eIF3d and eIF3e (133 promoted and 106 repressed) (Figure 1D). Moreover, the direction and degree of translational changes were concordant for mRNAs regulated by either eIF3e or eIF3d ($R^2 = 0.21$) (Figure S1G). While some overlap of transcripts regulated by eIF3d or eIF3e would be anticipated, as the KD of eIF3e decreased eIF3d protein levels, we also found eIF3e and eIF3d to regulate distinct transcripts. We identified transcripts regulated by both eIF3d and eIF3e, as well as transcripts regulated specifically by either eIF3d or eIF3e, and visualized the representative transcripts (Figure 1E). We identified similar pathways enriched or depleted for TE changes upon eIF3e and eIF3d depletion (Data S1). Interestingly, mRNAs encoding proteins in the “hypoxia” hallmark gene set were significantly enriched with eIF3e KD and to a lesser extent with eIF3d KD (Figure 1F).

eIF3e and eIF3d are necessary for the acute translational hypoxic response

Given the enrichment of the hypoxia hallmark gene set (Figure 1F) and that both eIF3d and eIF3e potentiate various stress responses,[14,15,25,52–54] we examined their role in the hypoxic response. Because the tumor-promotional roles of hypoxia have largely been attributed to the transcriptional response downstream of HIF1α,[4,55] we first asked if eIF3d or eIF3e influences HIF1α expression in response to hypoxic conditions (4 h at 1% O_2). The hypoxia-dependent increase of HIF1α protein levels was significantly attenuated by the depletion of either eIF3d or eIF3e in multiple cell lines, including two metastatic breast cancer cell lines (MCF7-SIX1[47] and MDA-MB-231) and the immortalized human embryonic kidney cell line HEK293T (Figures 2A, 2B, and S2A). We further tested whether eIF3d and eIF3e are involved in the translational response to hypoxia in two different metastatic breast cancer cell lines. Specifically, we performed Ribo-seq in MCF7-SIX1 and MDA-MB-231 cells ± eIF3d or eIF3e KD under acute hypoxic (1% O_2 for 1 h) vs. normoxic conditions. We chose an early time point after hypoxia induction (1 h) to examine the translational changes that occur prior to the many anticipated transcriptional changes downstream of hypoxia-dependent HIF1α induction. RNA-seq and Ribo-seq replicates were again highly correlated in these experiments (Figures S2B–S2D). Acute hypoxia led to many hundreds more mRNAs with statistically significant changes in RPFs compared to RNA levels in both MCF7-SIX1 (Figure 2C) and MDA-MB-231 (Figure 2D) cells. Particularly for MCF7-SIX1 cells, more mRNAs exhibited a loss, rather than a gain, of RPFs, consistent with diminished canonical translation reported in hypoxia[56] (Figure 2C). We identified 358 and 544 mRNAs exhibiting statistically significant changes in TE after 1 h of hypoxia in MCF7SIX1 and MDA-MB231 cells, respectively (Table S1). Strikingly, this acute translational hypoxic response was abolished with eIF3e KD and eIF3d KD (Figures 2E and 2G) in MCF7-SIX1 cells. The acute translational hypoxic response was also significantly inhibited with eIF3e KD and eIF3d KD in the MDA-MB-231 cells (Figures 2F and 2H). While we observed decreases in HIF1α protein levels with eIF3d and eIF3e KD at the 1-h time point (Figures S2E and S2F), the TE for HIF1α did not change, indicating that eIF3d/3e do not directly regulate HIF1α translation in acute hypoxia (Figures S2G and S2H). We conclude that translation is the major early form of gene regulation in response to acute oxygen deprivation and that eIF3e and eIF3d are required for this acute translational hypoxic response and hypoxia-dependent HIF1α induction in multiple contexts.

We next turned our attention to the full scope of mRNAs regulated by eIF3d and eIF3e in both hypoxic and normoxic conditions rather than solely those mRNAs in the acute translational hypoxic response. Depletion of eIF3d and eIF3e altered the translation of specific subsets of mRNAs, as opposed to globally impacting translation, in both conditions and cell lines (Figures S2I and S2J), ranging from as few as 224 mRNAs (eIF3d KD in normoxic MDA-MB-231 cells) to as many as 1526 mRNAs (eIF3d KD in hypoxic MCF7-SIX1 cells). Interestingly, eIF3d KD resulted in more mRNAs translationally regulated in hypoxia than normoxia for both cell lines, indicating enhanced activity of eIF3d in response to hypoxia. Compared to normoxia, we also observed more mRNAs regulated by eIF3e in hypoxia for MCF7-SIX1 cells but not for MDA-MB-231 cells. Indeed, we observed a statistically significant overlap for both eIF3d- and eIF3e-regulated mRNAs between cell lines in both normoxia (Figures S2K and S2L) and hypoxia (Figures 2I and 2J). To validate our Ribo-seq, we examined the changes in protein levels for several of these overlapping mRNAs whose translation requires eIF3e and eIF3d in hypoxia in both MCF7SIX1 and MDA-MB-231 cell lines. Specifically, we focused on *RB1CC1*, *TEAD1*, and *PCBP2*, which all exhibited decreased TE upon eIF3d and eIF3e KD in hypoxic conditions. As expected, depletion of eIF3d and eIF3e decreased the protein levels for all three targets after 4 h of hypoxia (Figures 2K and 2L). These data robustly demonstrate that eIF3d and eIF3e control the translation of a similar, but not identical, subset of mRNAs in multiple breast cancer cell lines and that eIF3d activity, in particular, is potentiated by hypoxia.

eIF3e and eIF3d regulate induction of hypoxia and hypoxia-induced invasion

Since eIF3e and eIF3d are required for the acute translational hypoxic response, we wanted to explore the functional consequence of their loss to hypoxia-associated phenotypes. To this end, we utilized a previously developed hypoxia fate-mapping (HFM) system cultured in 3D.[57] In this system, MDA-MB-231 cells were transduced with two plasmids that enable the cells to permanently switch from expressing dsRed during normoxic conditions to expressing GFP during hypoxic conditions.[57] This fluorescent switch is controlled by a Cre recombinase that is transcriptionally regulated via a promoter containing HIF-responsive elements (HREs). Therefore, Cre is only able to cut out the dsRed gene and allow GFP expression when HIF1α is induced in hypoxic conditions.[57] We refer to the HFM cells as 231HFM. To enable hypoxia to occur in a more natural setting, we embedded the 231HFM tumorspheres in a mixture of Matrigel and collagen. Over time, we observed that the tumorspheres formed a hypoxic core, as evidenced by the induction of GFP (Figure 3A). As anticipated due to reductions in HIF1α levels (Figure 2B), both eIF3d and eIF3e KD decreased the ratio of GFP/RFP observed in the tumorspheres over time (Figures 3A and 3B). Importantly, we also observed that eIF3d KD and eIF3e KD decreased tumorsphere invasion, when examined over time (Figure 3C). These data are of interest, as the hypoxic response has been linked to invasion.[58] In line with this finding, our data show that the GFP/dsRed ratio is significantly correlated with increased invasion (Figure 3D) and that this correlation is lost with both eIF3e and eIF3d KD. These data demonstrate that eIF3e and eIF3d are necessary to mediate the invasive phenotype in response to hypoxia.

The gene signatures associated with eIF3e and eIF3d predict poor prognosis in patients with breast cancer

Hypoxia is known to promote tumor progression and correlate with worse prognosis among patients with breast cancer.[4,55,59] Since our data show that eIF3d and eIF3e promote the hypoxic response in breast cancer cells, we asked whether *EIF3D* or *EIF3E* was dysregulated in large breast cancer patient cohorts, such as METABRIC and TCGA, in a manner correlated with survival. We found that 46% and 61% of patients exhibited gain/amplification in *EIF3E* alleles in the METABRIC and TCGA datasets, respectively (Figures S3A and S3B). In addition, only 4% and 11% of patients exhibited gain/amplification in *EIF3D* alleles in the METABRIC and TCGA datasets, respectively (Figures S3A and S3B). Interestingly, in the METABRIC dataset, *EIF3E* gain/amplification significantly correlated with worse prognosis, while *EIF3D* gain/amplification did not (Figures 4A and 4B). Although the amplification of neither *EIF3E* nor *EIF3D* significantly correlated with prognosis in the TCGA dataset, there is a trend of *EIF3E* amplification correlating with worse prognosis (Figures S3C and S3D). However, since the chromosomal location of *EIF3E* (8q23) is very close to that of *cMYC* (8q24), which is often amplified in many human malignancies and acts as a prominent oncogene,[60] the prognostic value of EIF3E may be driven by *cMYC* co-amplification. Therefore, we developed RNA-seq signatures for *EIF3D* and *EIF3E* using the intersection of genes with statistically significant changes in expression with eIF3d or eIF3e KD in hypoxia ($p < 0.05$ and log2 fold change [LFC] >1 or <−1) in MCF7SIX1 cells and MDA-MB-231 cells to identify a prognostic signature specific to *EIF3D* and *EIF3E* independent of *cMYC*. We stratified patients from the METABRIC and TCGA datasets based on the enrichment of *EIF3D* and *EIF3E* RNA signatures. Enrichment of the *EIF3E* signature was associated with worsened survival compared to patients depleted of the *EIF3E* signature in both the METABRIC and TCGA datasets (Figures 4C and S3E). The eIF3d signature also correlated with overall survival in both datasets, albeit with a smaller hazard ratio (HR), indicating the lower predictive value of the *EIF3D* signature (Figures 4D and S3F).

Next, we were interested in the relative contribution of the hypoxia and *EIF3D/E* signatures to worsened patient survival. We started by stratifying patients using a previously published 42-gene mRNA hypoxia signature conserved across breast cancer cell lines.[61] As expected, enrichment of the hypoxia signature was associated with worsened patient survival in the METABRIC dataset[62–64] (Figure S3G). Next, we grouped patients into four categories based on high or low hypoxia and high or low eIF3d/e signature enrichment (Figure S3H). The groups with high eIF3e signature enrichment had worse survival outcomes than groups with low eIF3e signature enrichment for both the low-hypoxia (low 3e-low hypoxia vs. high 3e-low hypoxia; HR: 1.43, $p < 0.001$) and high-hypoxia (low-high vs. high-high; HR: 1.36, $p < 0.012$) groups. This result suggests that eIF3e contributes to worse survival outcomes together with and in addition to hypoxia (Figure 4E). This was not the case for eIF3d; worse prognosis appeared to be driven by the hypoxia signature rather than the eIF3d signature (Figures 4F and S3I). Together, these data provide compelling evidence for the value of targeting eIF3e in breast cancer.

Small molecules targeting eIF3e

We previously demonstrated that a small molecule, NCGC00378430 (abbreviated 8430), reduces metastasis in an MCF7-SIX1 xenograft model.[48] While 8430 decreased the interaction between SIX1 and EYA2 (two known tumor-promotional proteins), we also observed that levels of both proteins were decreased, and thus the direct target of this molecule remained unclear.[48] To identify the direct target of 8430, we performed isothermal shift assays (ITSAs) on cells treated with 8430 or a vehicle control (DMSO) and found that eIF3e was the most significantly stabilized protein in the presence of 8430 (Figure 5A). To independently confirm stabilization of eIF3e with 8430, we performed cellular thermal shift assays (CETSAs) on MCF7-SIX1 lysates and found that 8430 stabilized eIF3e at 53°C, while other eIF3 subunits were not stabilized (Figure 5B). After this discovery, we synthesized closely related compounds to 8430 and found that an analog compound (209) also stabilizes eIF3e in CETSAs (Figure 5B). We then performed isothermal dose-response fingerprint (ITDRF) experiments, in which a dose-response curve is generated to calculate half-maximal effective concentrations (EC_{50} s). The calculated EC_{50} s are 13.6 and 18.3 μM for 8430 and 209, respectively (Figures 5C–5F). These data suggest that 8430 and 209 bind to eIF3e and provide a potential explanation for the prevention of metastasis by 8430,[48] via inhibition of eIF3e.

Pharmacologic inhibition of eIF3e inhibits the acute translational hypoxic response

To determine whether our novel class of eIF3e-targeting small molecules inhibit eIF3e-associated hypoxic responses, we first looked at HIF1α levels after decreasing O_2 levels to 1% for 4 h, with and without 8430 and 209 treatment. As observed with both eIF3d and eIF3e KD, treatment of both MCF7-SIX1 and HEK293T cells with 8430 and 209 led to reduced HIF1α induction in response to hypoxia (Figures 6A and 6B). Given the promising similarities, we performed Ribo-seq in normoxic or hypoxic conditions for 1 h ± treatment with DMSO (vehicle) or compound 209, which was chosen due to the larger reduction of HIF1α levels when compared to 8430 (Figures 6A and 6B). RNA-seq and Ribo-seq replicates were again highly correlated in normoxia ($R = 0.99$ and $R = 0.93$, respectively) and hypoxia ($R = 0.99$ and $R = 0.95$, respectively) (Figures S4A and S4B). As observed previously in our siCtrl cells (Figure 2E), acute hypoxia caused many changes in ribosomal footprints, with minimal changes to transcript levels, indicating translation as the major regulatory response at this time point (Figure 6C). In line with our eIF3e-KD results (Figures 2E and 2F), the acute hypoxic translational response was largely ablated in MCF7-SIX1 breast cancer cells treated with 209 (Figure 6D). Similarly, we identified more mRNAs with significantly changed TEs after 209 treatment in hypoxic conditions when compared to normoxic conditions (Figure 6E). Neither the RNA levels nor RPFs for HIF1α changed in response to 209, again suggesting that eIF3e does not directly regulate the translation of HIF1α (Figure S4C). Interestingly, no significant overlap was observed between mRNAs translationally regulated by 209 treatment and those regulated by eIF3e or eIF3d in normoxic conditions (Figure 6F). In contrast, we observed a highly significant overlap between mRNAs regulated by eIF3e and 209 in hypoxic conditions (Figure 6G, blue), whereas eIF3d and 209 showed a more moderate, yet significant, overlap with specifically the downregulated mRNAs in hypoxic conditions (Figure 6G, yellow). These results further suggest that our compound is on target and inhibits eIF3e function.

Similar experiments with 8430 (Figures S4D–S4G) also resulted in inhibition of the acute translational hypoxia response (Figure S4F) without altering the expression or translation of HIF1α (Figure S4G). Taken together, our data demonstrate that there is a unique, eIF3e translational mechanism in hypoxia that can be specifically inhibited pharmacologically with a small molecule targeting eIF3e.

Pharmacologic inhibition of eIF3e prevents hypoxic-related invasion

Because our novel eIF3e-targeting compounds inhibited HIF1α induction and selective translation in response to acute hypoxia, we again utilized the 231HFM tumorsphere model to determine whether hypoxia-induced phenotypes could be pharmacologically inhibited. Since the tumorsphere assays take place over a week, we assessed the stability of both 8430 and 209 over time. Our data demonstrate that compound 209 degrades over time in our culture media, whereas 8430 is stable over the 7 days used in our tumorsphere assays (Figures S5A and S5B). Thus, we used 8430 to examine whether pharmacological targeting of eIF3e could inhibit hypoxia-induced phenotypes in 3D over time. Importantly, 8430 significantly decreased the GFP:dsRed ratio within these tumorspheres over time (Figures 7A and 7B), similar to eIF3e KD. Furthermore, 8430 decreased tumorsphere invasion over the time course of this assay (Figure 7C). The GFP:dsRed ratio was highly correlated with invasion for DMSO-treated cells ($R = 0.96$) and was much lower for 8430 treatment ($R = 0.47$) (Figure 7D), indicating that 8430 leads to a decoupling between HIF1α activity and invasion. These data demonstrate the ability of the eIF3e-targeting compound (8430) to functionally inhibit hypoxia-induced invasion and provide further evidence that 8430 is acting on target given the similarities to eIF3e KD.

Response to additional cellular stressors requires eIF3e and eIF3d and can be inhibited with our novel eIF3e-targeting compounds

Because we demonstrate a role for both eIF3e and eIF3d in the hypoxic response and because both molecules have been implicated in response to a variety of stressors,[14,15,25,52–54] we further explored whether eIF3d and eIF3e are cooperating to regulate additional stress-induced responses and whether our eIF3e-targeting small molecule could inhibit these responses. Of interest, we observed that eIF3e *and* eIF3d both promoted the TE of the *ATF4* mRNA, a known master transcriptional regulator of the integrated stress response (ISR),[65,66] in our original Ribo-seq experiment under normoxic conditions (Figure 1E). To further explore the role of eIF3e and eIF3d in regulating ATF4 protein expression, we treated a variety of cell lines with thapsigargin (TG) or tunicamycin (TM)—two potent inducers of the ISR[17]—to induce ATF4 translation. We verified that the induction of ATF4 is abrogated with both eIF3e KD and eIF3d KD in multiple cell lines (Figures S6A and S6B). Of note, we noticed abnormally high levels of ATF4 basally in our MCF7-SIX1 cells. We found that these cells were uniquely sensitive to siRNA transfection, which activated the ISR (Figure S6C). This finding likely explains why we found ATF4 to be an mRNA translationally regulated by eIF3e and eIF3d KD without the addition of an ER stressor. Other cell lines that were less sensitive to siRNA transfection also retained loss of ATF4 in both eIF3e- and eIF3d-KD cell lines after TG and TM treatment. Importantly, both 8430 and 209 also significantly attenuated the induction of ATF4 expression after TG treatment in MCF7SIX1 cells, similar to eIF3d KD and eIF3e KD, and after TM treatment in the MCF7-SIX1 cells

(Figures S6D and S6E). Similar results were observed in the MDA-MB-231 model with 8430/209 + TG; however, reduction of ATF4 did not occur in the 8430/209 + TM-treated conditions. Taken together, these data demonstrate that 8430 and 209 can inhibit other stress-responsive phenotypes dependent upon eIF3e.

DISCUSSION

In this study, we demonstrate that eIF3d and eIF3e are required for cancer cells to respond to hypoxia through regulating a selective translational program and that this translational program is critical for the induction of HIF1α and the phenotypic response to hypoxia. We further demonstrate that eIF3e and eIF3d RNA signatures are associated with poor overall survival in patients with breast cancer. Importantly, we have developed first-in-class compounds that target eIF3e and inhibit the acute translational hypoxic response, resulting in reduced invasion in response to hypoxia. As we have previously demonstrated that one of these novel compounds inhibits metastasis *in vivo*,[48] our results suggest that our first-in-class inhibitors may reduce metastasis at least in part by altering the response to hypoxia through eIF3e.

Hypoxia is a well-known stressor that can promote tumor progression and metastasis.[4,55,67] During stress, cells often downregulate mTOR signaling, thus diminishing canonical eIF4F-mediated translation. However, a subset of mRNAs is still translated via non-canonical translation programs, which is thought to be vital to cellular adaptation. However, the hypoxia-induced mechanism by which non-canonical translation is mediated remains underexplored. Herein, we find that selective translational regulation by eIF3d and eIF3e is critical for the initial response to hypoxia. Interestingly, eIF3d, which can bind the 7-methylguanosine mRNA cap,[14,23] consistently regulated the translation of more mRNAs in hypoxia compared to normoxia. It is tempting to speculate that the enhanced eIF3d regulatory capacity could be due to opportunistic cap binding in acute hypoxia when eIF4E cap binding is attenuated by inhibition of mTOR activity.[68,69] Future work will determine the precise mechanism of the enhanced translational regulation by eIF3d in hypoxia and whether that is the case for other oncogenic stressors, making eIF3d a promising target for preferential targeting of cancer cells.

This translational response precedes the well-defined pleiotropic transcriptional response of HIF1α—which is attributed to the tumor-promotional effects of hypoxia. Furthermore, hypoxia-induced HIF1α accumulation is abrogated by the loss of eIF3d and eIF3e, suggesting that inhibition of the hypoxic translational response will also attenuate further downstream HIF1α-mediated transcriptional responses. Interestingly, we did not observe changes in *HIF1α* mRNA or RPFs with loss of eIF3d or eIF3e, suggesting that the change in HIF1α downstream of eIF3d and eIF3e is a function of altered protein stability. Furthermore, we did not see significant changes in HIF1α regulators such as Von Hippel-Lindau (VHL) protein—the main regulator of HIF1α stability.[70] Interestingly, two studies discovered that eIF3b, another subunit within the eIF3 complex, can directly bind to proteins to prevent their ubiquitination and subsequent degradation.[29,71] However, it is currently unknown whether this eIF3b-mediated stabilization extends to other VHL targets, such as HIF1α, or whether other eIF3 subunits—such as eIF3d or eIF3e—are required. Although

our study did not uncover a direct translational effect of eIF3d or eIF3e on HIF1α, a previous report demonstrated that eIF3e loss results in decreased *HIF1*α translation in glioblastoma cells.[16,54] However, this study utilized a hypoxia mimetic, $CoCl_2$, to stabilize HIFα proteins rather than low oxygen levels, which may account for the differences in regulation of HIF1α observed when compared to our study. Furthermore, it is possible that HIF1α is translationally regulated at a later time point (>1 h).

Our work expands on previous studies that have found a selective eIF3d-dependent translational response that occurs when various stressors (glucose deprivation and ISR activators) inhibit canonical translation, allowing translation of a subset of mRNAs—such as cJUN and ATF4—to promote survival.[14–16,72] Furthermore, eIF3e has been shown to promote resistance to radiotherapy and is overexpressed in patients with recurrent glioblastoma tumors post-radiotherapy, suggesting that eIF3e is required for adapting to this stress.[54] These data add to the mounting evidence for the crucial role of these translation factors for adaptation to a wide variety of stressors, including microenvironmental stressors and current therapies.

In line with the critical role of eIF3e/d in stress responses, we found that our eIF3e- and eIF3d-associated RNA signatures, as well as a previously described hypoxia RNA signature,[61] both predict poor prognosis in breast cancer datasets. When taken together with our observation that eIF3d and eIF3e KD inhibit pro-metastatic phenotypes such as invasion, these findings underscore the potential value of developing small molecules to target eIF3e as a novel therapeutic strategy. In our current study, we demonstrate that novel small-molecule compounds, 8430 and 209, stabilize eIF3e but not other eIF3 components, suggesting that they specifically bind eIF3e. These compounds recapitulate phenotypes seen in eIF3e KD cells, such as preventing the acute translational hypoxic response, HIF1α induction, HIF1α-mediated dsRed:GFP switch, and invasion in 3D, further suggesting these compounds are on target. Importantly, we have previously shown that 8430 can inhibit metastasis in our *in vivo* MCF7-SIX1 xenograft model.[48] In that work, we demonstrated that 8430 reduced the expression of a pro-metastatic transcription factor, SIX1, and its cofactor, EYA2, respectively. 8430 was able to reverse SIX1-mediated transcriptional changes, SIX1-and TGFβ-induced EMT, and SIX1-induced metastasis.[48] However, we did not observe a decrease in the TE of SIX1 or EYA2 with eIF3e KD or with 209 or 8430 treatment, suggesting that eIF3e indirectly regulates these pro-metastatic transcription factors. Nevertheless, it is exciting that 8430 targets eIF3e and inhibits metastasis *in vivo*. To conclusively demonstrate that our eIF3e-targeting compounds are reducing metastasis through eIF3e specifically, it will be important to perform genetic experiments in which eIF3e is depleted and animals are treated *in vivo* with 8430. Also, future biophysical studies are needed to identify the precise mechanism of action of our compounds on eIF3e and to further optimize the compounds to improve drug-like characteristics, such as potency and pharmacokinetic parameters. Nonetheless, our compounds can serve as tools to understand the function of eIF3e in various cellular contexts.

In addition to hypoxia, tumor cells encounter countless other stressors that are constantly fluctuating as they proliferate, deplete resources, and metastasize throughout the body.[73] During these times of cellular stress, tumor cells are in a state of vulnerability and must

adapt to survive. The ability of tumor cells to adapt engenders a plasticity that is challenging to target therapeutically.[5,6,74] Therefore, identifying commonalities between mechanisms of adaptation to various stressors and exploiting these vulnerabilities could enable the development of novel therapeutic strategies for targeting cancer cells at multiple stages of tumor progression, including metastasis.[75] Devising novel means to inhibit selective translation may be one such approach. Indeed, many studies have shown the importance of mRNA translation for tumor plasticity and progression.[5,74,76] To this end, various translation inhibitors have been developed but have limited use in the clinic, often due to toxicity or a lack of efficacy.[77,78] However, the development of strategies to specifically inhibit stress-induced translation—which is generally highly active in malignant tissues—could uncover key vulnerabilities to limit tumor plasticity with minimal toxicities. Our studies and others provide a growing body of literature that suggests that IF3d and eIF3e are critical for adaptation to a variety of different stressors,[14,15,25,52–54] indicating that these proteins are viable therapeutic targets, potentially through small-molecule inhibitors such as those we have developed for eIF3e.

Limitations of the study

Our current study is focused on the early translational response to stress after 1 h of hypoxia. Important alterations to mRNA translation likely occur throughout the adaptation to the stressor. Since tumor cells are constantly exposed to chronic and acute stressors, it will be important to understand the mechanisms and phenotypic outcomes of adapting to these stressors after the initial insult in future studies. Furthermore, in the absence of spike-ins for normalization, we may underestimate the extent of global translational alterations in our experiment, which could be expected during acute hypoxia. Although we found that eIF3e and eIF3d are required for the acute translational response during hypoxia and tumor cell invasion, the direct role of eIF3e or eIF3d in metastasis remains unknown. Future *in vivo* studies will elucidate the metastatic roles of eIF3e and eIF3d.

RESOURCE AVAILABILITY

Lead contact

Requests for further information and resources should be directed to and will be fulfilled by the lead contact, Neelanjan Mukherjee (neelanjan.mukherjee@cuanschutz.edu).

Materials availability

Compound 209 generated in this study will be made available after the completion of a materials transfer agreement.

Data and code availability

- The RNA-seq and Ribo-seq data have been deposited at SRA as GSE307666 and are publicly available.
- The pipeline and all downstream analysis, which was performed in R with custom scripts, are available at https://github.com/mukherjeelab/2024_eIF3e_hypoxia/ and https://zenodo.org/records/17316520.

- Any additional information required to analyze the data reported in this paper is available from the lead contact (Neelanjan Mukherjee) upon request.

STAR★METHODS

EXPERIMENTAL MODEL AND STUDY PARTICIPANT DETAILS

Cell lines and cell culture: Cells were cultured in incubators at 37°C with 5% CO_2 and ~21% O_2 (atmospheric). MCF7SIX1 cells (Clone A13) (derived from human female breast cancer cells) were generated as previously described.[47] The MDA-MB-231 Hypoxia fate-mapping cells (derived from human female breast cancer cells) were a generous gift from Dr. Daniele Gilkes.[57] HEK293T cells (derived from human female embryonic kidney cells) were acquired from the University of Colorado Anschutz Medical Campus Cell Technology shared resource. The MCF7SIX1 and HEK293T cells were cultured Dulbecco's High Glucose Modified Eagle Medium (DMEM, Hyclone SH30022.01), with which 10% fetal bovine serum (FBS, Corning 35–010-CV), and 2 mM L-glutamine (L-glut, Hyclone SH30034.02) were supplemented. The MDA-MB-231 cells were cultured with Dulbecco's High Glucose Modified Eagle Medium (DMEM, Hyclone SH30022.01), with which 5% fetal bovine serum (FBS, Corning 35–010-CV), 2 mM L-glutamine (L-glut, Hyclone SH30034.02), were supplemented. All cell lines were STR profiled at the end of the study to ensure identity and were also tested for mycoplasma every 6 months with the MycoAlert Mycoplasma Detection Kit (Lonza LT07–118). Cell lines were passaged after thawing prior to use in experiments and were re-thawed periodically. 8430 and 209 were resuspended in DMSO to a working solution concentration of 20 mM. All experiments with 8430 and 209 were used at 20 μM (1:1000 dilution) with DMSO as a vehicle control. TG and TM were used at 100 nM and 2.5 mg/mL, respectively, with DMSO as a vehicle control.

METHOD DETAILS

siRNA transfections: ON-TARGET*plus* siRNA SMARTPools were ordered specifically for eIF3e (cat #: L-010518–00-0010) and eIF3d (cat #: L-017556–00-0010) from Horizon Discovery. ON-TARGET*plus* non-targeting pool (cat # D-001810–10) was always used as a control. siRNA transfections occurred in 25% OPTIMEM Reduced serum media and 75% full growth media (cat # 31985062). siRNAs were added to the media mixture at a concentration of 7.5 nM for 5 min prior to the addition of 1.875 mL Lipofectamine RNAI MAX transfection reagent (cat # 13778150) per 1 mL of media. siRNA:lipofectamine mixtures were incubated for 20 min before adding it directly onto the cell culture overnight. siRNA knockdowns were assessed 48–72 h after the addition of the siRNAs.

Western Blotting: Cells were washed with PBS then either frozen in the plate (dry) or lysed fresh with RIPA buffer. Cells were detached and whole-cell protein extracts were isolated by lysing cell pellets using RIPA buffer. Collected protein lysates (30–60 μg) were separated using polyacrylamide gel electrophoresis, and size-separated proteins were then transferred to methanol-activated PVDF membranes followed by the blocking step using 5% non-fat milk in TBST (20 mM Tris HCl, pH 7.5, 150 mM NaCl, 0.1% Tween 20). Next, membranes were incubated with indicated primary antibodies (1:1000) overnight at 4°C. The following day, membranes were washed with TBST and secondary antibodies

(1:5000) were applied in 5% non-fat milk in TBST. Finally, membranes were washed and examined using chemiluminescence followed by imaging using the Odyssey Fc Imaging System (LI-COR Biosciences) or the Azure 600 Gel imaging system (Azure biosystems).

RNA-seq and ribosome profiling: Ribosome profiling was performed as described previously with a few modifications.[88] The lysis buffer contained 100 μg/mL cycloheximide. Following lysis and clarification by centrifugation, total RNA was quantified using the Qubit RNA BR assay kit. A portion of the lysate was reserved as input sample for RNASeq preparation. Total RNA was extracted using the DirectZol RNA Microprep kit (ZYMO Research) following the manufacturer's instructions with on-column DNase I treatment. Ribosomal RNA was depleted from total RNA using our previously described RNaseH-based method,[89] then input into the KAPA RNA Hyper prep RNAseq library prep kit (Roche) according to manufacturer's instructions with dual-index adapters, followed by quality check of the final libraries by Qubit dsDNA HS assay and Tapestation High Sensitivity D1000 screentape. Libraries were pooled and submitted for paired-end 150 bp sequencing on the Illumina NovaSeq6000 platform to a depth of 40 million paired end reads per library.

The remaining lysate was used as input into the ribosome footprinting reaction with 750 U RNase I (Invitrogen Ambion). The digestion was stopped with SUPERaseIN followed by recovery of monosomes with equilibrated Microspin S-400 HR (GE) columns. Trizol LS was added to the monosome-containing elution and RNA isolated with the ZYMO Directzol microprep kit with on-column DNase I treatment. The isolated RNA was depleted of rRNA using the siTOOLs riboPOOLs kit for ribosome profiling. The samples were resolved on a 15% TBE-Urea PAGE gel and ribosome protected fragments (RPFs) 28–29 nt in size were extracted and recovered. RPFs were treated with T4-PNK then used as input into the Qiagen QIAseq miRNA library prep kit with provided single index adapters. Libraries were pooled and submitted for paired-end 150 bp sequencing on the Illumina NovaSeq 6000 S4 platform to a depth of 50 million paired end reads per library (Novogene Corporation Inc.). Adapters were trimmed with Cutadapt.[83] UMIs were trimmed and collapsed using UMI-tools.[84] Salmon[85] was used for quantifying transcript levels from RNA-seq and Ribo-seq libraries using GENCODEv26 transcriptome assembly. Briefly, Salmon data were imported using the tximport.[79] Transcript expression was quantified using Salmon v1.6 (12). Quality of ribosome sequencing data, including ribosome footprint length, p-site positioning, and three-nucleotide periodicity, was assessed using Ribowaltz.[90] All RNA-seq and Ribo-seq reads were compared using Pearson correlation, by which an outlier was identified and removed from downstream analysis (Hypoxia, si3e, Rep B, RNA-seq). Differential expression and translation was calculated using the deltaTE approach.[51] The odds ratio and *p*-value for the overlap between genes was performed using a Fisher's exact test. The pipeline and all downstream analysis, which was performed in R with custom scripts, are available at https://github.com/mukherjeelab/2024_eIF3e_hypoxia/.

Hypoxic conditions: To provide a hypoxic environment, cells were placed in either a modular hypoxic chamber and filled with a premixed gas comprised of 1% O_2, or the cells were placed in a BioSpherix hypoxic chamber flushed with N_2 and CO_2 gas. The O2 and

CO2 concentrations in the BioSpherix chamber were maintained at 1% and 5%, respectively, using a carbon dioxide & oxygen controller (BioSpherix). These conditions were maintained constant throughout the course of the experiments. After hypoxic incubation was completed, quick lysis (<3 min) of the cells was necessary to prevent reoxygenation from affecting our results.

Event-free survival analysis and eIF3e/eIF3d/hypoxia signatures: eIF3e and eIF3d RNA signatures were generated by comparing the change in mRNAs levels in siCtrl cells compared to KD cells in hypoxia in MCF7-SIX1 and MDA-MB-231 cells. Genes included in each signature had a $\log_2$ fold change <−1 or >1 and an adjusted p value < 0.05 in both cell lines, i.e., the intersection. The hypoxia signature was obtained from Ye et al., 2018,[61] and patients were stratified by enrichment of the signature. mRNA microarray data for 2509 primary breast tumor samples were downloaded from cBioPortal for Cancer Genomics[91,92] from the METABRIC Breast Cancer Study.[62,63] Duplicate microarray data for patient entries were merged by taking the mean of the Z score for each gene. Patients with missing microarray data were removed. After preprocessing, we performed downstream analysis on the remaining 1980 patients. mRNA sequencing data for 1102 primary breast tumor samples were obtained from The Cancer Genome Atlas (TCGA) project and downloaded from cBioPortal for Cancer Genomics.[91–93] After deduplicating and matching to clinical data, 1083 samples were included in downstream analyses.

For copy number variation analysis, patients from the METABRIC Breast Cancer Study were grouped by eIF3e or eIF3d copy number. For signature analysis for both METABRIC and TCGA cohorts, patients were assigned to groups based on the top quartile of enrichment (top 25%METABRIC n = 495, TCGA n = 275) and bottom quartile of enrichment i.e., depletion (bottom 25% n = 495, TCGA n = 275) for a given signature. To determine statistical differences between groups, each group was compared to the lowest expression group (e.g., no CNA for eIF3e, het CNA loss for eIF3d; bottom 25% for signatures). Statistics were calculated using a Cox proportional hazards regression analysis.

Tumorsphere assays: 8,000 231HFM cells were plated in each well of a 96-well ULA round bottom plate (Corning cat#7007), centrifuged for 3 min at 150 G, then incubated overnight. For the siRNA KD experiments, these were plated 24 h after siRNA transfection. For 8430 experiments, 8430 (or DMSO) was added to the tumorspheres at time of plating. Matrigel (Corning cat#354234) (10mg/mL) was thawed and kept on ice. Matrigel was mixed 1:1 with full growth media (addition of DMSO or 8430 was added, if applicable). Then, rat tail Collagen I (Corning cat#354249) was added to either 10% total volume (for KD experiments) or 3% of the total volume (8430 experiments) and mixed thoroughly. This mixture of matrigel, media, collagen was carefully pipetted down the side of the wells without disturbing the tumorsphere, then incubated at 37°C for 45 min to solidify. Additionally full growth media (with 8430 or DMSO, if applicable), was added on top of the solidified matrigel pad. The plate was then added to the incucyte SX5 (sartorius) for images to be taken at 4x over time. The green and orange optical module were used to measure the fluorescence of the GFP and dsRed, respectively. The brightfield optical module was used for total spheroid size and invasion area.

Isothermal shift assays: Full description provided in supplemental information. Cell lysates were prepared by suspending frozen cell pellets in 1 mL of lysis buffer: phosphate-buffered saline supplemented with 0.4% Igepal CA-630, a 1X cOmplete Mini EDTA-free Protease Inhibitor Cocktail (Sigma #11836170001), and 1X Pierce Phosphatase Inhibitor (Thermo Fisher Scientific #A32957), adjusted to pH 7.4. Cells were lysed through sonication. The lysate was then centrifuged at 21,000 g for 15 min at 4°C, and the supernatant was collected. Protein concentration was quantified using a bicinchoninic acid (BCA) assay (Thermo Fisher Scientific, Waltham, MA), and the lysate was standardized to a concentration of 5 mg/mL. Cell lysates were treated with compound 8430 at a final concentration of 20 μM, with DMSO adjusted to a 1% final concentration. A vehicle control containing only 1% DMSO was simultaneously prepared.

Isothermal proteome profiling using was performed using the ITSA method, as previously described.[94] A 40 μL aliquot of lysate was dispensed into individually sealable PCR wells (4titude Random Access plate, PN 4ti-0960/RA). The sample plate was equilibrated to room temperature for 2 min, sealed and positioned in the thermal cycler for a 3-min incubation at a constant temperature of 53°C. The plate was then immediately cooled to 4°C, followed by centrifugation at 500*g* for 2 min to remove condensation.

Protein aggregates were pelleted by transferring PCR tubes to 1.5 mL microcentrifuge tubes and centrifuging at 21,000 g for 30 min at 4°C. Supernatants were carefully transferred to fresh low-retention tubes. Protein samples were denatured and cysteines alkylated by adding 50 μL of denaturing buffer (8 M guanidine HCl, 100 mM HEPES (pH 8.5), 10 mM TCEP, and 40 mM 2-chloroacetamide) and heating samples to 90°C for 10 min. After cooling to ambient temperature, 400 μL of cold acetone was added and samples incubated overnight at −20°C.

Samples were centrifuged at 21,000 g for 30 min at −10°C. Acetone wash steps were performed twice using 80% cold acetone, with intermediate sonication in a Bioruptor at 4°C. Acetone pellets were dried and resuspended in a digestion master mix: 10% trifluoroethanol, 50 mM HEPES (pH 8.5), Lys-C (2 μg, Wako #129–02541), and trypsin (2 μg, Sigma #T6567). Samples were suspended by sociation and digested for 16 h at 37°C with constant agitation (1,200 rpm) using an Eppendorf Thermal Mixer C. Peptide labeling utilized the 10-plex TMT reagents (Thermo Fisher Scientific #90110) according to manufacturer protocols.

Peptides were fractionated using an Agilent 1100 HPLC. Mass spectrometric analysis utilized a Waters M-class Acquity system coupled with an Orbitrap Fusion (Thermo Scientific). Peptides were separated using a gradient elution from 3% to 85% acetonitrile over 121 min. MS2 spectra were collected using data-dependent acquisition with specified resolution and AGC parameters. Raw mass spectrometry files were processed using MaxQuant (version 1.6.3.323) with the Andromeda search engine. Searches were conducted against an UniProt human protein database, implementing stringent peptide identification criteria. Quantitative analysis employed R (version 3.5.2) with the limma package. Data preprocessing included filtering, quantile normalization, and statistical analysis using linear modeling and empirical Bayes methods. Multiple testing correction was performed using the Benjamini-Hochberg procedure to control false discovery rate.

Cellular thermal shift assay (CETSA) and isothermal dose-response fingerprint (IDRF) CETSA: MCF7SIX1 cells were grown to 95% confluency and trypsinized for 5 min at 37°C, neutralized with FBS-containing media and pelleted at 1,000 RPM for 10 min at 4°C. Cell pellets containing 1.2×10^6 cells were incubated on ice for 30 min with 100 μL of lysis buffer containing 50 mM pH 7.5 Tris, 100 mM NaCl, 1 mM DTT, and protease inhibitor cocktail (Thermo Scientific). The cell pellets were then lysed by pulling them through a 23G syringe needle 8 times. Lysed cells were centrifuged at 15,000 RPM for 30 min at 4°C and the supernatant collected. Lysate was treated with either 20 μM of compound in DMSO or 2% DMSO (CETSA) or a serial dilution of compound concentrations (ITDRF CETSA) for 10 min at room temperature. The cell lysate was heated at 53°C for 3 min in a thermocycler or incubated at 0°C on ice and rotated briefly on a microtube rotator to bring down the condensation on the side of the tube. The samples were then transferred to low-adhesion 1.5 mL tubes and centrifuged at 15,000 RPM for 1 h at 4°C. 30 μL of supernatant was collected from each tube. Western blots were performed on the resulting supernatants using the following antibodies: α-GAPDH (mouse, GeneTex GT239), α-eIF3a (rabbit, Bethyl A302–002A), α-eIF3b (rabbit, Bethyl A301–760A), α-eIF3c (rabbit, Bethyl A300377A), α-eIF3d (rabbit, Bethyl A301–758A), α-eIF3e (rabbit, Bethyl A302–984A), α-eIF3k (rabbit, Bethyl A301–762A), and α-eIF3l (rabbit, Bethyl A304–754A).

Comparative studies of stability between 8430 and 209

Thin-layer chromatography (TLC): TLC was carried out on a silica plate with 10% ethyl acetate-hexane solvent system. 8430 and 209 were treated with buffer for 1, 5, and 7 days and checked for decomposition after extraction with sodium bicarbonate dichloromethane.

Quantitative NMR (qNMR): qNMR was used to investigate how much pure 8430 and 209 were present in the buffer solution. Ethelyne carbonate (13 mg for 209, 11 mg for 8430) was considered as internal standard, d 4.49 in DMSO-D6 and 4.54 in CDCl3. For 8430 qNMR analysis, d 7.20 was considered to be the analyte chemical shift with 2.03 integration, whereas d 3.11 was considered with 4.00 integration for 8430 qNMR analysis.

Synthesis of 8430 and 209: Detailed description in supplemental information.

QUANTIFICATION AND STATISTICAL ANALYSIS

There are many different statistical tests used in the study, and each is defined in the legend for the respective figure panel. For quantitative and statistical analysis of genomic datasets, we recommend users access our code through either GitHub (https://github.com/mukherjeelab/2024_eIF3e_hypoxia/) or Zenodo (https://zenodo.org/records/17316520). All statistical analysis were conducted with R or GraphPad Prism.

Supplementary Material

Refer to Web version on PubMed Central for supplementary material.

ACKNOWLEDGMENTS

We thank Dexiang Gao for guidance with statistical analyses and Dr. Daniele Gilkes for the HFM system (231HFM cells). This work was supported by National Institutes of Health grants R35GM147025 (N.M.), R35GM145289 (R.Z.), R01 CA224867 (H.L.F. and M.T.L.), CA301267 (H.L.F. and R.Z.), R35 GM142774 (M.C.C.), NRSA T32CA174648 (C.A.), 5T32CA190216-08 (S.C.P.), T32-GM136444 (K.M.), and 1F31CA275314-01A1 (A.W.); Dan L. Duncan Comprehensive Cancer Center, Baylor College of Medicine (BCM), grants P30CA125123 and RP170691 (MTL); and Cancer League of Colorado grant AWD-242679-NM (N.M. and H.L.F.). This work used the Cell Technologies (RRID: SCR_021982) and Biostatistics and Bioinformatics Shared Resource (RRID: SCR_021983), supported by P30CA046934.

REFERENCES

1. Gross S, Rahal R, Stransky N, Lengauer C, and Hoeflich KP (2015). Targeting cancer with kinase inhibitors. J. Clin. Investig. 125, 1780–1789. 10.1172/JCI76094. [PubMed: 25932675]
2. Society AC (2024). Cancer Facts and Figures 2024 (American Cancer Society).
3. Valastyan S, and Weinberg RA (2011). Tumor metastasis: molecular insights and evolving paradigms. Cell 147, 275–292. 10.1016/j.cell.2011.09.024. [PubMed: 22000009]
4. Rankin EB, and Giaccia AJ (2016). Hypoxic control of metastasis. Science 352, 175–180. 10.1126/science.aaf4405. [PubMed: 27124451]
5. Fabbri L, Chakraborty A, Robert C, and Vagner S (2021). The plasticity of mRNA translation during cancer progression and therapy resistance. Nat. Rev. Cancer 21, 558–577. 10.1038/s41568-021-00380-y. [PubMed: 34341537]
6. Lee LJ, Papadopoli D, Jewer M, Del Rincon S, Topisirovic I, Lawrence MG, and Postovit LM (2021). Cancer Plasticity: The Role of mRNA Translation. Trends Cancer 7, 134–145. 10.1016/j.recan.2020.09.005. [PubMed: 33067172]
7. Cammas A, Desprairies A, Dassi E, and Millevoi S (2024). The shaping of mRNA translation plasticity by RNA G-quadruplexes in cancer progression and therapy resistance. NAR Cancer 6, zcae025. 10.1093/narcan/zcae025. [PubMed: 38828391]
8. Robichaud N, Sonenberg N, Ruggero D, and Schneider RJ (2019). Translational Control in Cancer. Cold Spring Harb. Perspect. Biol. 11, a032896. 10.1101/cshperspect.a032896. [PubMed: 29959193]
9. Hsieh AC, Liu Y, Edlind MP, Ingolia NT, Janes MR, Sher A, Shi EY, Stumpf CR, Christensen C, Bonham MJ, et al. (2012). The translational landscape of mTOR signalling steers cancer initiation and metastasis. Nature 485, 55–61. 10.1038/nature10912. [PubMed: 22367541]
10. Micalizzi DS, Ebright RY, Haber DA, and Maheswaran S (2021). Translational Regulation of Cancer Metastasis. Cancer Res. 81, 517–524. 10.1158/0008-5472.CAN-20-2720. [PubMed: 33479028]
11. Jackson RJ, Hellen CUT, and Pestova TV (2010). The mechanism of eukaryotic translation initiation and principles of its regulation. Nat. Rev. Mol. Cell Biol. 11, 113–127. 10.1038/nrm2838. [PubMed: 20094052]
12. Mir DA, Ma Z, Horrocks J, and Rogers A (2024). Stress-Induced Eukaryotic Translational Regulatory Mechanisms. J. Clin. Med. Sci. 8, 1000277. [PubMed: 39364184]
13. Vaupel P, Mayer A, and Höckel M (2004). Tumor hypoxia and malignant progression. Methods Enzymol. 381, 335–354. 10.1016/S0076-6879(04)81023-1. [PubMed: 15063685]
14. Lamper AM, Fleming RH, Ladd KM, and Lee ASY (2020). A phosphorylation-regulated eIF3d translation switch mediates cellular adaptation to metabolic stress. Science 370, 853–856. 10.1126/science.abb0993. [PubMed: 33184215]
15. Mukhopadhyay S, Amodeo ME, and Lee ASY (2023). eIF3d controls the persistent integrated stress response. Mol. Cell 83, 3303–3313.e6. 10.1016/j.molcel.2023.08.008. [PubMed: 37683648]
16. Herrmannova A, Jelínek J, Pospíšilová K, Kerényi F, Vomastek T, Watt K, Brábek J, Mohammad MP, Wagner S, Topisirovic I, et al. (2024). Perturbations in eIF3 subunit stoichiometry alter expression of ribosomal proteins and key components of the MAPK signaling pathways. eLife 13, RP95846. 10.7554/eLife.95846. [PubMed: 39495207]

17. Guan BJ, van Hoef V, Jobava R, Elroy-Stein O, Valasek LS, Cargnello M, Gao XH, Krokowski D, Merrick WC, Kimball SR, et al. (2017). A Unique ISR Program Determines Cellular Responses to Chronic Stress. Mol. Cell 68, 885–900.e6. 10.1016/j.molcel.2017.11.007. [PubMed: 29220654]

18. Aitken CE, Beznosková P, Vlčkova V, Chiu WL, Zhou F, Valášek LS, Hinnebusch AG, and Lorsch JR (2016). Eukaryotic translation initiation factor 3 plays distinct roles at the mRNA entry and exit channels of the ribosomal preinitiation complex. eLife 5, e20934. 10.7554/eLife.20934. [PubMed: 27782884]

19. Eliseev B, Yeramala L, Leitner A, Karuppasamy M, Raimondeau E, Huard K, Alkalaeva E, Aebersold R, and Schaffitzel C (2018). Structure of a human cap-dependent 48S translation pre-initiation complex. Nucleic Acids Res. 46, 2678–2689. 10.1093/nar/gky054. [PubMed: 29401259]

20. Gomes-Duarte A, Lacerda R, Menezes J, and Romão L (2018). eIF3: a factor for human health and disease. RNA Biol. 15, 26–34. 10.1080/15476286.2017.1391437. [PubMed: 29099306]

21. Hinnebusch AG (2006). eIF3: a versatile scaffold for translation initiation complexes. Trends Biochem. Sci. 31, 553–562. 10.1016/j.tibs.2006.08.005. [PubMed: 16920360]

22. Lee ASY, Kranzusch PJ, and Cate JHD (2015). eIF3 targets cell-proliferation messenger RNAs for translational activation or repression. Nature 522, 111–114. 10.1038/nature14267. [PubMed: 25849773]

23. Lee AS, Kranzusch PJ, Doudna JA, and Cate JHD (2016). eIF3d is an mRNA cap-binding protein that is required for specialized translation initiation. Nature 536, 96–99. 10.1038/nature18954. [PubMed: 27462815]

24. Shah M, Su D, Scheliga JS, Pluskal T, Boronat S, Motamedchaboki K, Campos AR, Qi F, Hidalgo E, Yanagida M, and Wolf DA (2016). A Transcript-Specific eIF3 Complex Mediates Global Translational Control of Energy Metabolism. Cell Rep. 16, 1891–1902. 10.1016/j.celrep.2016.07.006. [PubMed: 27477275]

25. Zhou C, Arslan F, Wee S, Krishnan S, Ivanov AR, Oliva A, Leatherwood J, and Wolf DA (2005). PCI proteins eIF3e and eIF3m define distinct translation initiation factor 3 complexes. BMC Biol. 3, 14. 10.1186/1741-7007-3-14. [PubMed: 15904532]

26. Li B, Xiong X, Xu J, Peng D, Nie G, Wen N, Wang Y, and Lu J (2024). METTL3-mediated m(6)A modification of lncRNA TSPAN12 promotes metastasis of hepatocellular carcinoma through SENP1-depentent deSUMOylation of EIF3I. Oncogene 43, 1050–1062. 10.1038/s41388-024-02970-0. [PubMed: 38374407]

27. Choudhuri A, Maitra U, and Evans T (2013). Translation initiation factor eIF3h targets specific transcripts to polysomes during embryogenesis. Proc. Natl. Acad. Sci. USA 110, 9818–9823. 10.1073/pnas.1302934110. [PubMed: 23716667]

28. Fraser CS, Berry KE, Hershey JWB, and Doudna JA (2007). eIF3j is located in the decoding center of the human 40S ribosomal subunit. Mol. Cell 26, 811–819. 10.1016/j.molcel.2007.05.019. [PubMed: 17588516]

29. Huang R, Nie W, Mi L, Yao C, and Zhu H (2024). EIF3B stabilizes PCNA by counteracting SYVN1-mediated ubiquitination to serve as a promotor in cholangiocarcinoma. Aging (Albany NY) 16, 7311–7330. 10.18632/aging.205759. [PubMed: 38687509]

30. Huo C, Wu D, Li X, Zhang Y, Hu B, Zhang T, Ren J, Wang T, and Liu Y (2024). eIf3a mediates malignant biological behaviors in colorectal cancer through the PI3K/AKT signaling pathway. Cancer Biol. Ther. 25, 2355703. 10.1080/15384047.2024.2355703. [PubMed: 38782896]

31. Jin H, Huang X, Pan Q, Ma N, Xie X, Wei Y, Yu F, Wen W, Zhang B, Zhang P, et al. (2024). The EIF3H-HAX1 axis increases RAF-MEK-ERK signaling activity to promote colorectal cancer progression. Nat. Commun. 15, 2551. 10.1038/s41467-024-46521-3. [PubMed: 38514606]

32. Chong PSY, Chooi JY, Lim SLJ, Chung TH, Brunmeir R, Leow ACY, Toh SHM, Balan K, Azaman MIB, Wu Z, et al. (2024). Epigenetic dysregulation of eukaryotic initiation factor 3 subunit E (eIF3E) by lysine methyltransferase REIIBP confers a pro-inflammatory phenotype in t(4;14) myeloma. Haematologica 109, 1893–1908. 10.3324/haematol.2023.283467. [PubMed: 38124661]

33. Alard A, Katsara O, Rios-Fuller T, Parra C.d.l., Ozerdem U, Ernlund A, and Schneider RJ. (2023). Breast cancer cell mesenchymal transition and metastasis directed by DAP5/eIF3d-mediated selective mRNA translation. Cell Rep. 42, 112646. 10.1016/j.celrep.2023.112646. [PubMed: 37314929]

34. Sesen J, Casaos J, Scotland SJ, Seva C, Eisinger-Mathason TSK, and Skuli N (2017). The Bad, the Good and eIF3e/INT6. Front. Biosci. 22, 1–20. 10.2741/4469.
35. Miyazaki S, Imatani A, Ballard L, Marchetti A, Buttitta F, Albertsen H, Nevanlinna HA, Gallahan D, and Callahan R (1997). The chromosome location of the human homolog of the mouse mammary tumor-associated gene INT6 and its status in human breast carcinomas. Genomics 46, 155–158. 10.1006/geno.1997.4996. [PubMed: 9403073]
36. Marchetti A, Buttitta F, Pellegrini S, Bertacca G, and Callahan R (2001). Reduced expression of INT-6/eIF3-p48 in human tumors. Int. J. Oncol. 18, 175–179. 10.3892/ijo.18.1.175. [PubMed: 11115556]
37. Gillis LD, and Lewis SM (2013). Decreased eIF3e/Int6 expression causes epithelial-to-mesenchymal transition in breast epithelial cells. Oncogene 32, 3598–3605. 10.1038/onc.2012.371. [PubMed: 22907435]
38. Desnoyers G, Frost LD, Courteau L, Wall ML, and Lewis SM (2015). Decreased eIF3e Expression Can Mediate Epithelial-to-Mesenchymal Transition through Activation of the TGFbeta Signaling Pathway. Mol. Cancer Res. 13, 1421–1430. 10.1158/1541-7786.MCR-14-0645. [PubMed: 26056130]
39. Suo J, Medina D, Herrera S, Zheng ZY, Jin L, Chamness GC, Contreras A, Gutierrez C, Hilsenbeck S, Umar A, et al. (2015). Int6 reduction activates stromal fibroblasts to enhance transforming activity in breast epithelial cells. Cell Biosci. 5, 10. 10.1186/s13578-015-0001-6. [PubMed: 25774287]
40. Grzmil M, Rzymski T, Milani M, Harris AL, Capper RG, Saunders NJ, Salhan A, Ragoussis J, and Norbury CJ (2010). An oncogenic role of eIF3e/INT6 in human breast cancer. Oncogene 29, 4080–4089. 10.1038/onc.2010.152. [PubMed: 20453879]
41. Li Z, Lin S, Jiang T, Wang J, Lu H, Tang H, Teng M, and Fan J (2014). Overexpression of eIF3e is correlated with colon tumor development and poor prognosis. Int. J. Clin. Exp. Pathol. 7, 6462–6474. [PubMed: 25400724]
42. Yong ZWE, Zaini ZM, Kallarakkal TG, Karen-Ng LP, Rahman ZAA, Ismail SM, Sharifah NA, Mustafa WMW, Abraham MT, Tay KK, and Zain RB (2014). Genetic alterations of chromosome 8 genes in oral cancer. Sci. Rep. 4, 6073. 10.1038/srep06073. [PubMed: 25123227]
43. Sesen J, Cammas A, Scotland SJ, Elefterion B, Lemarié A, Millevoi S, Mathew LK, Seva C, Toulas C, Moyal ECJ, and Skuli N (2014). Int6/eIF3e is essential for proliferation and survival of human glioblastoma cells. Int. J. Mol. Sci. 15, 2172–2190. 10.3390/ijms15022172. [PubMed: 24481065]
44. Batie M, and Rocha S (2020). Gene transcription and chromatin regulation in hypoxia. Biochem. Soc. Trans. 48, 1121–1128. 10.1042/BST20191106. [PubMed: 32369557]
45. Abou Khouzam R, Sharda M, Rao SP, Kyerewah-Kersi SM, Zeinelabdin NA, Mahmood AS, Nawafleh H, Khan MS, Venkatesh GH, and Chouaib S (2023). Chronic hypoxia is associated with transcriptomic reprogramming and increased genomic instability in cancer cells. Front. Cell Dev. Biol. 11, 1095419. 10.3389/fcell.2023.1095419. [PubMed: 36968212]
46. Yfantis A, Mylonis I, Chachami G, Nikolaidis M, Amoutzias GD, Paraskeva E, and Simos G (2023). Transcriptional Response to Hypoxia: The Role of HIF-1-Associated Co-Regulators. Cells 12, 798. 10.3390/cells12050798. [PubMed: 36899934]
47. Ford HL, Kabingu EN, Bump EA, Mutter GL, and Pardee AB (1998). Abrogation of the G2 cell cycle checkpoint associated with overexpression of HSIX1: a possible mechanism of breast carcinogenesis. Proc. Natl. Acad. Sci. USA 95, 12608–12613. 10.1073/pnas.95.21.12608. [PubMed: 9770533]
48. Zhou H, Blevins MA, Hsu JY, Kong D, Galbraith MD, Goodspeed A, Culp-Hill R, Oliphant MUJ, Ramirez D, Zhang L, et al. (2020). Identification of a Small-Molecule Inhibitor That Disrupts the SIX1/EYA2 Complex, EMT, and Metastasis. Cancer Res. 80, 2689–2702. 10.1158/0008-5472.CAN-20-0435. [PubMed: 32341035]
49. Ingolia NT, Ghaemmaghami S, Newman JRS, and Weissman JS (2009). Genome-wide analysis in vivo of translation with nucleotide resolution using ribosome profiling. Science 324, 218–223. 10.1126/science.1168978. [PubMed: 19213877]

50. Wagner S, Herrmannová A, Šikrová D, and Valášek LS (2016). Human eIF3b and eIF3a serve as the nucleation core for the assembly of eIF3 into two interconnected modules: the yeast-like core and the octamer. Nucleic Acids Res. 44, 10772–10788. 10.1093/nar/gkw972. [PubMed: 27924037]
51. Chothani S, Adami E, Ouyang JF, Viswanathan S, Hubner N, Cook SA, Schafer S, and Rackham OJL (2019). deltaTE: Detection of Translationally Regulated Genes by Integrative Analysis of Ribo-seq and RNA-seq Data. Curr. Protoc. Mol. Biol. 129, e108. 10.1002/cpmb.108. [PubMed: 31763789]
52. Thompson L, Depledge DP, Burgess HM, and Mohr I (2022). An eIF3d-dependent switch regulates HCMV replication by remodeling the infected cell translation landscape to mimic chronic ER stress. Cell Rep. 39, 110767. 10.1016/j.celrep.2022.110767. [PubMed: 35508137]
53. Mahe M, Rios-Fuller T, Katsara O, and Schneider RJ (2024). Non-canonical mRNA translation initiation in cell stress and cancer. NAR Cancer 6, zcae026. 10.1093/narcan/zcae026. [PubMed: 38828390]
54. Bertorello J, Sesen J, Gilhodes J, Evrard S, Courtade-Saïdi M, Augustus M, Uro-Coste E, Toulas C, Moyal ECJ, Seva C, et al. (2020). Translation reprogramming by eIF3 linked to glioblastoma resistance. NAR Cancer 2, zcaa020. 10.1093/narcan/zcaa020. [PubMed: 34316689]
55. Wicks EE, and Semenza GL (2022). Hypoxia-inducible factors: cancer progression and clinical translation. J. Clin. Investig. 132, e159839. 10.1172/JCI159839. [PubMed: 35642641]
56. Koritzinsky M, Magagnin MG, van den Beucken T, Seigneuric R, Savelkouls K, Dostie J, Pyronnet S, Kaufman RJ, Weppler SA, Voncken JW, et al. (2006). Gene expression during acute and prolonged hypoxia is regulated by distinct mechanisms of translational control. EMBO J. 25, 1114–1125. 10.1038/sj.emboj.7600998. [PubMed: 16467844]
57. Godet I, Shin YJ, Ju JA, Ye IC, Wang G, and Gilkes DM (2019). Fate-mapping post-hypoxic tumor cells reveals a ROS-resistant phenotype that promotes metastasis. Nat. Commun. 10, 4862. 10.1038/s41467-019-12412-1. [PubMed: 31649238]
58. Emami Nejad A, Najafgholian S, Rostami A, Sistani A, Shojaeifar S, Esparvarinha M, Nedaeinia R, Haghjooy Javanmard S, Taherian M, Ahmadlou M, et al. (2021). The role of hypoxia in the tumor microenvironment and development of cancer stem cell: a novel approach to developing treatment. Cancer Cell Int. 21, 62. 10.1186/s12935-020-01719-5. [PubMed: 33472628]
59. Ye Y, Hu Q, Chen H, Liang K, Yuan Y, Xiang Y, Ruan H, Zhang Z, Song A, Zhang H, et al. (2019). Characterization of Hypoxia-associated Molecular Features to Aid Hypoxia-Targeted Therapy. Nat. Metab. 1, 431–444. 10.1038/s42255-019-0045-8. [PubMed: 31984309]
60. Duffy MJ, O'Grady S, Tang M, and Crown J (2021). MYC as a target for cancer treatment. Cancer Treat Rev. 94, 102154. 10.1016/j.ctrv.2021.102154. [PubMed: 33524794]
61. Ye IC, Fertig EJ, DiGiacomo JW, Considine M, Godet I, and Gilkes DM (2018). Molecular Portrait of Hypoxia in Breast Cancer: A Prognostic Signature and Novel HIF-Regulated Genes. Mol. Cancer Res. 16, 1889–1901. 10.1158/1541-7786.MCR-18-0345. [PubMed: 30037853]
62. Pereira B, Chin SF, Rueda OM, Vollan HKM, Provenzano E, Bardwell HA, Pugh M, Jones L, Russell R, Sammut SJ, et al. (2016). The somatic mutation profiles of 2,433 breast cancers refines their genomic and transcriptomic landscapes. Nat. Commun. 7, 11479. 10.1038/ncomms11479. [PubMed: 27161491]
63. Rueda OM, Sammut SJ, Seoane JA, Chin SF, Caswell-Jin JL, Callari M, Batra R, Pereira B, Bruna A, Ali HR, et al. (2019). Dynamics of breast-cancer relapse reveal late-recurring ER-positive genomic subgroups. Nature 567, 399–404. 10.1038/s41586-019-1007-8. [PubMed: 30867590]
64. Curtis C, Shah SP, Chin SF, Turashvili G, Rueda OM, Dunning MJ, Speed D, Lynch AG, Samarajiwa S, Yuan Y, et al. (2012). The genomic and transcriptomic architecture of 2,000 breast tumours reveals novel subgroups. Nature 486, 346–352. 10.1038/nature10983. [PubMed: 22522925]
65. Iurlaro R, and Muñoz-Pinedo C (2016). Cell death induced by endoplasmic reticulum stress. FEBS J. 283, 2640–2652. 10.1111/febs.13598. [PubMed: 26587781]
66. Vasudevan D, Neuman SD, Yang A, Lough L, Brown B, Bashirullah A, Cardozo T, and Ryoo HD (2020). Translational induction of ATF4 during integrated stress response requires noncanonical initiation factors eIF2D and DENR. Nat. Commun. 11, 4677. 10.1038/s41467-020-18453-1. [PubMed: 32938929]

67. Donato C, Kunz L, Castro-Giner F, Paasinen-Sohns A, Strittmatter K, Szczerba BM, Scherrer R, Di Maggio N, Heusermann W, Biehlmaier O, et al. (2020). Hypoxia Triggers the Intravasation of Clustered Circulating Tumor Cells. Cell Rep. 32, 108105. 10.1016/j.celrep.2020.108105. [PubMed: 32905777]
68. Connolly E, Braunstein S, Formenti S, and Schneider RJ (2006). Hypoxia inhibits protein synthesis through a 4E-BP1 and elongation factor 2 kinase pathway controlled by mTOR and uncoupled in breast cancer cells. Mol. Cell Biol. 26, 3955–3965. 10.1128/MCB.26.10.3955-3965.2006. [PubMed: 16648488]
69. Yanagiya A, Suyama E, Adachi H, Svitkin YV, Aza-Blanc P, Imataka H, Mikami S, Martineau Y, Ronai ZA, and Sonenberg N (2012). Translational homeostasis via the mRNA cap-binding protein, eIF4E. Mol. Cell 46, 847–858. 10.1016/j.molcel.2012.04.004. [PubMed: 22578813]
70. Haase VH (2009). The VHL tumor suppressor: master regulator of HIF. Curr. Pharm. Des. 15, 3895–3903. 10.2174/138161209789649394. [PubMed: 19671042]
71. Tan J, Li X, Wang Y, Wang L, Zhao X, Wang Y, and Cui M (2025). EIF3B stabilizes MAP2K2 to activate the ERK pathway and promote the progression of laryngeal squamous cell carcinoma. Cell Death Discov. 11, 333. 10.1038/s41420-025-02634-2. [PubMed: 40691141]
72. Roiuk M, Neff M, and Teleman AA (2024). eIF4E-independent translation is largely eIF3d-dependent. Nat. Commun. 15, 6692. 10.1038/s41467-024-51027-z. [PubMed: 39107322]
73. Senft D, and Ronai ZA (2016). Adaptive Stress Responses During Tumor Metastasis and Dormancy. Trends Cancer 2, 429–442. 10.1016/j.trecan.2016.06.004.
74. Kong D, Hughes CJ, and Ford HL (2020). Cellular Plasticity in Breast Cancer Progression and Therapy. Front. Mol. Biosci. 7, 72. 10.3389/fmolb.2020.00072. [PubMed: 32391382]
75. Chen M, and Xie S (2018). Therapeutic targeting of cellular stress responses in cancer. Thorac. Cancer 9, 1575–1582. 10.1111/1759-7714.12890. [PubMed: 30312004]
76. Ebright RY, Lee S, Wittner BS, Niederhoffer KL, Nicholson BT, Bardia A, Truesdell S, Wiley DF, Wesley B, Li S, et al. (2020). Deregulation of ribosomal protein expression and translation promotes breast cancer metastasis. Science 367, 1468–1473. 10.1126/science.aay0939. [PubMed: 32029688]
77. Dmitriev SE, Vladimirov DO, and Lashkevich KA (2020). A Quick Guide to Small-Molecule Inhibitors of Eukaryotic Protein Synthesis. Biochemistry. 85, 1389–1421. 10.1134/S0006297920110097. [PubMed: 33280581]
78. Laham-Karam N, Pinto GP, Poso A, and Kokkonen P (2020). Transcription and Translation Inhibitors in Cancer Treatment. Front. Chem. 8, 276. 10.3389/fchem.2020.00276. [PubMed: 32373584]
79. Soneson C, Love MI, and Robinson MD (2015). Differential analyses for RNA-seq: transcript-level estimates improve gene-level inferences. F1000Res. 4, 1521. 10.12688/f1000research.7563.2. [PubMed: 26925227]
80. Wickham H, Averick M, Bryan J, Chang W, McGowan L, François R, Grolemund G, Hayes A, Henry L, Hester J, et al. (2019). Welcome to the tidyverse. J. Open Source Softw. 4, 1686.
81. Love MI, Huber W, and Anders S (2014). Moderated estimation of fold change and dispersion for RNA-seq data with DESeq2. Genome Biol. 15, 550. [PubMed: 25516281]
82. Langmead B, and Salzberg SL (2012). Fast gapped-read alignment with Bowtie 2. Nat. Methods 9, 357–359. [PubMed: 22388286]
83. Martin M (2011). Cutadapt removes adapter sequences from high-throughput sequencing reads. EMBnet. J. 17, 10. 10.14806/ej.17.1.200.
84. Smith T, Heger A, and Sudbery I (2017). UMI-tools: modeling sequencing errors in Unique Molecular Identifiers to improve quantification accuracy. Genome Res. 27, 491–499. 10.1101/gr.209601.116. [PubMed: 28100584]
85. Patro R, Duggal G, Love MI, Irizarry RA, and Kingsford C (2017). Salmon provides fast and bias-aware quantification of transcript expression. Nat. Methods 14, 417–419. 10.1038/nmeth.4197. [PubMed: 28263959]
86. Blighe K Publication-ready volcano plots with enhanced colouring and labeling. https://bioconductor.org/packages/release/bioc/html/EnhancedVolcano.html.

87. Kassambara A rstatix: Pipe-Friendly Framework for Basic Statistical Tests. R package version 0.7.2. https://rpkgs.datanovia.com/rstatix/.

88. Calviello L, Mukherjee N, Wyler E, Zauber H, Hirsekorn A, Selbach M, Landthaler M, Obermayer B, and Ohler U (2016). Detecting actively translated open reading frames in ribosome profiling data. Nat. Methods 13, 165–170. 10.1038/nmeth.3688. [PubMed: 26657557]

89. Baldwin A, Morris AR, and Mukherjee N (2021). An Easy, Cost-Effective, and Scalable Method to Deplete Human Ribosomal RNA for RNA-seq. Curr. Protoc. 1, e176. 10.1002/cpz1.176. [PubMed: 34165268]

90. Lauria F, Tebaldi T, Bernabò P, Groen EJN, Gillingwater TH, and Viero G (2018). riboWaltz: Optimization of ribosome P-site positioning in ribosome profiling data. PLoS Comput. Biol. 14, e1006169. 10.1371/journal.pcbi.1006169. [PubMed: 30102689]

91. Cerami E, Gao J, Dogrusoz U, Gross BE, Sumer SO, Aksoy BA, Jacobsen A, Byrne CJ, Heuer ML, Larsson E, et al. (2012). The cBio cancer genomics portal: an open platform for exploring multidimensional cancer genomics data. Cancer Discov. 2, 401–404. 10.1158/2159-8290.CD-12-0095. [PubMed: 22588877]

92. Gao J, Aksoy BA, Dogrusoz U, Dresdner G, Gross B, Sumer SO, Sun Y, Jacobsen A, Sinha R, Larsson E, et al. (2013). Integrative analysis of complex cancer genomics and clinical profiles using the cBioPortal. Sci. Signal. 6, pl1. 10.1126/scisignal.2004088. [PubMed: 23550210]

93. Cancer Genome Atlas Network (2012). Comprehensive molecular portraits of human breast tumours. Nature 490, 61–70. 10.1038/nature11412. [PubMed: 23000897]

94. Ball KA, Webb KJ, Coleman SJ, Cozzolino KA, Jacobsen J, Jones KR, Stowell MHB, and Old WM (2020). An isothermal shift assay for proteome scale drug-target identification. Commun. Biol. 3, 75. 10.1038/s42003-020-0795-6. [PubMed: 32060372]

Highlights

- Selective mRNA translation precedes the HIF-mediated transcriptional response to hypoxia
- eIF3e and eIF3d are required for the acute selective translational hypoxic response
- eIF3e and eIF3d gene signatures predict worse survival in patients with breast cancer
- eIF3e-mediated stress-induced translation can be inhibited by small molecules

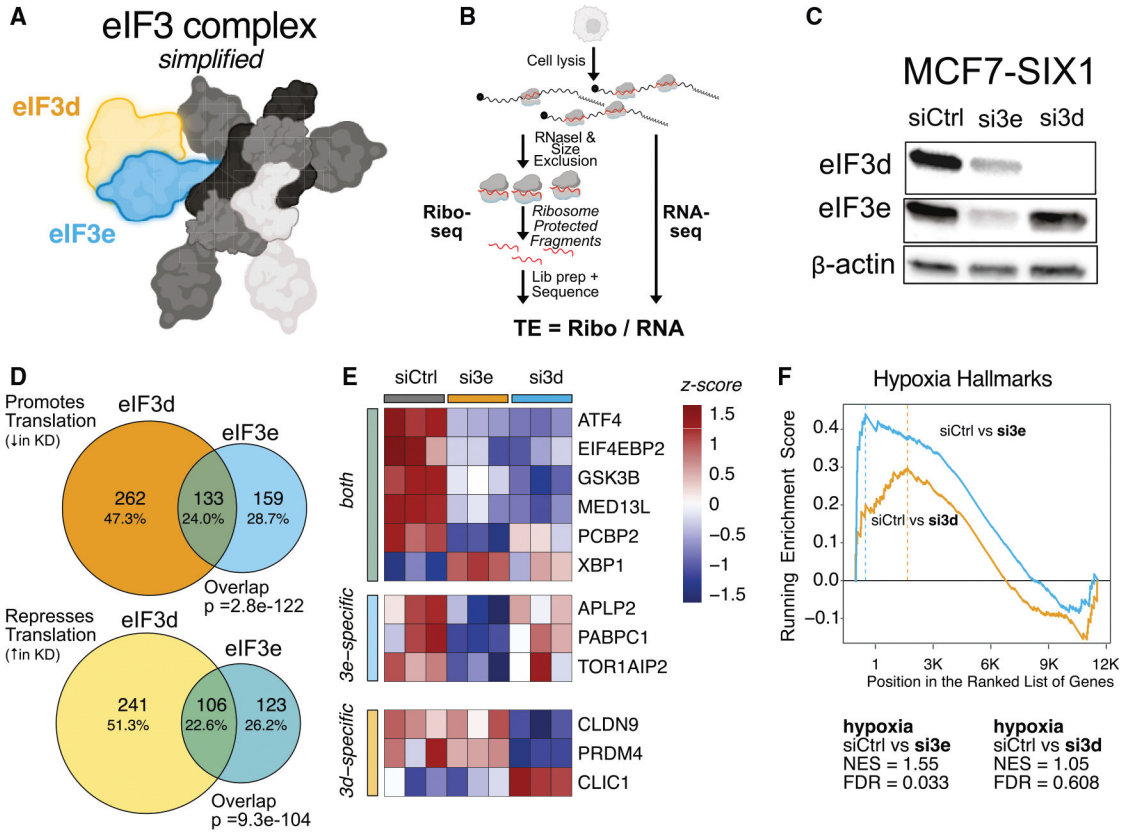

Figure 1. Overlapping and distinct functions of eIF3d and eIF3e

(A) Diagram of a simplified eIF3 complex with only eIF3d and eIF3e labeled for clarity.

(B) Outline of the experimental design of Ribo-seq and RNA-seq.

(C) siRNA knockdown (KD) of eIF3d and eIF3e in MCF7-SIX1 cells, followed by western blot analysis.

(D) Venn diagram of the overlapping and distinct differentially translated mRNAs after eIF3d and eIF3e KD. *p* values were calculated with Fisher's exact test.

(E) Heatmap of specific mRNAs that are shared or specific to eIF3d vs. eIF3e. The values are *Z* scores of the TE.

(F) Gene set enrichment analysis for the hypoxia hallmark dataset when eIF3e and eIF3d are knocked down.

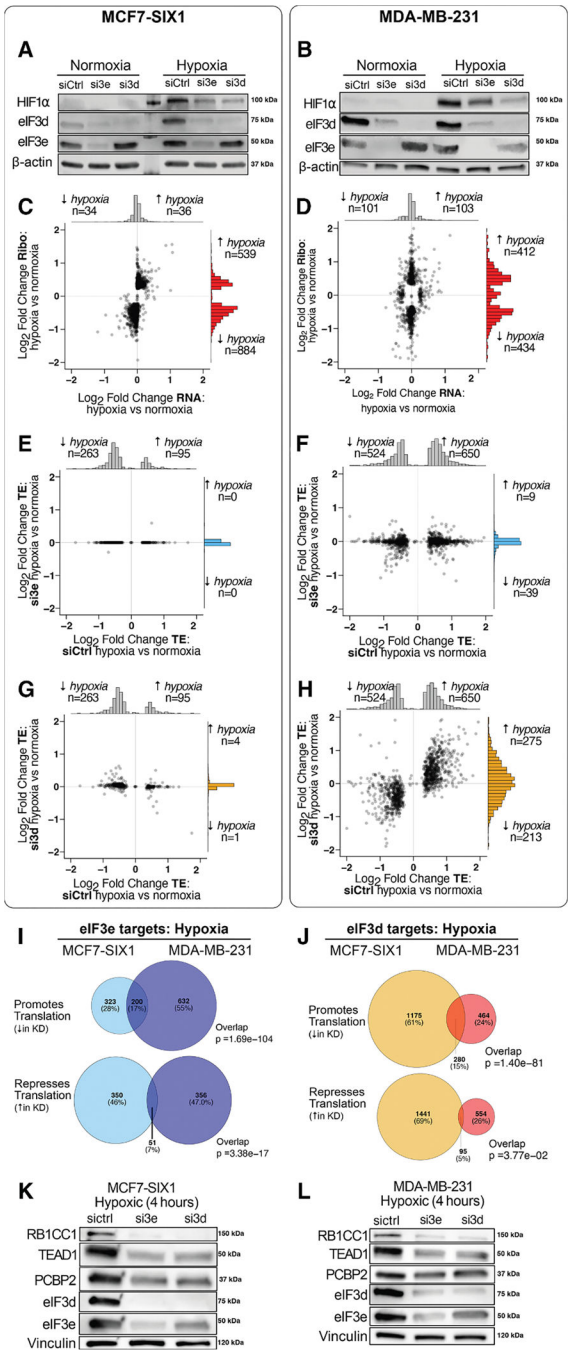

Figure 2. eIF3e and eIF3d are required for the acute translational hypoxic response

(A and B) Western blot analysis of HIF1α after eIF3d and eIF3e knockdown (KD) in normoxic and hypoxic (4 h at 1% O2) conditions in (A) MCF7-SIX1 and (B) MDA-MB-231 cells.

(C and D) Log_2 fold changes of RPFs (*y* axis) and RNA levels (*x* axis) comparing siCtrl cells in normoxia vs. hypoxia in (C) MCF7-SIX1 and (D) MDA-MB-231 cells. Only mRNAs with a statistically significant difference (adjusted *p* value [adj *p*] < 0.05) are shown.

(E–H) Comparison of TE changes from normoxia to hypoxia in (E) MCF7-SIX1 and (F) MDA-MB-231 siCtrl cells (x axis) vs. si3e cells (y axis) or (G and H) si3d cells (y axis). Only mRNAs with a statistically significant TE difference (adj $p < 0.05$) are shown.
(I and J) Venn diagram showing the overlap of mRNAs with statistically significant TE changes in MCF7-SIX1 and MDA-MB-231 for (I) eIF3e KD or (J) eIF3d KD.
(K and L) Western blot analysis of high-confidence targets in (K) MCF7-SIX1 and (L) MDA-MB-231 cells.

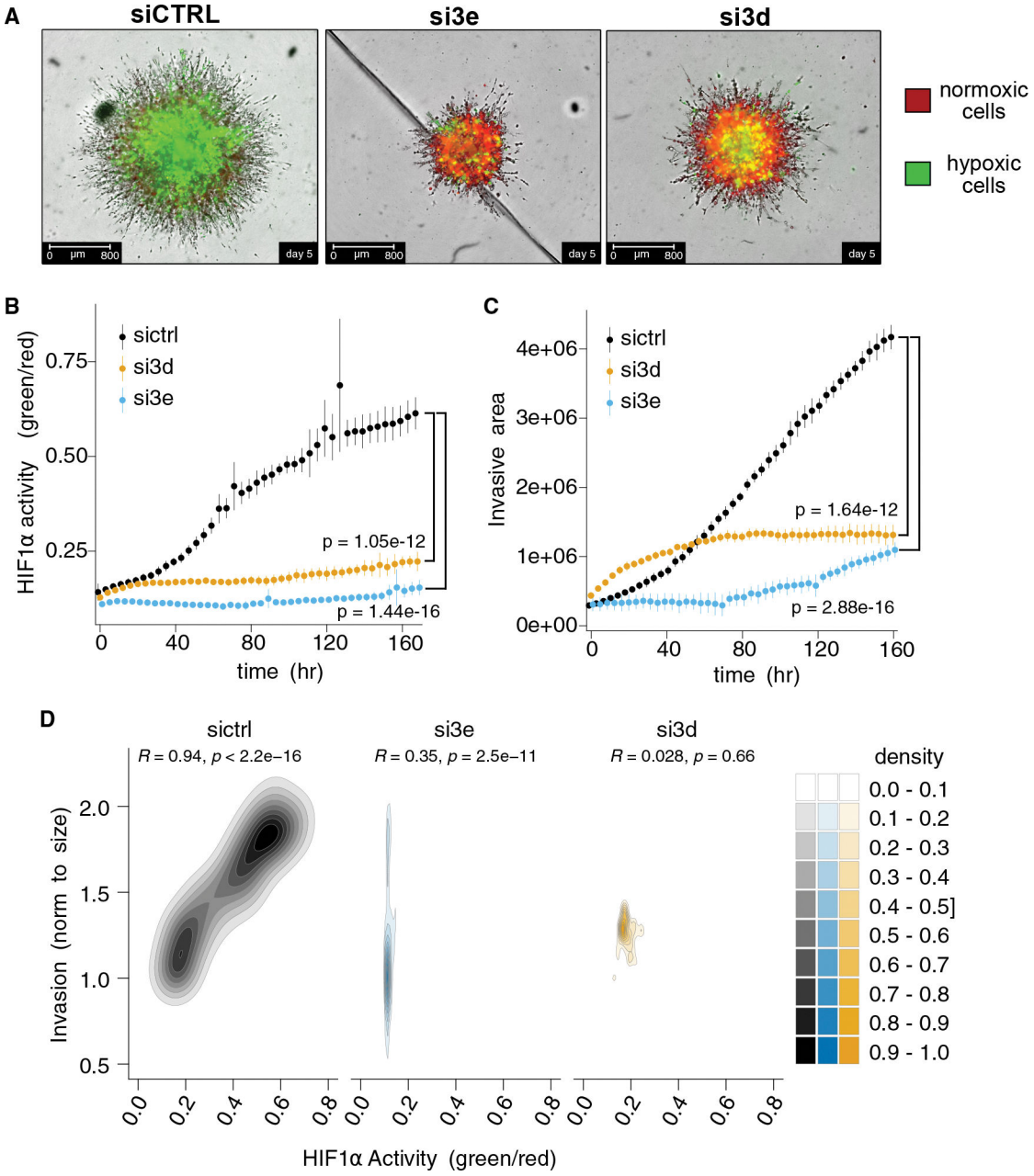

Figure 3. Loss of eIF3d and eIF3d decreases HIF1α-mediated effects and tumorsphere invasion

(A) Representative images of 231HFM cells grown in tumorspheres embedded in Matrigel and collagen I ± eIF3d and eIF3e KD.

(B) Fluorescence ratio of GFP:dsRed over time ± eIF3d and eIF3e KD.

(C) Invasive area of the 231 tumorspheres over time ± eIF3d and eIF3e KD.

For (B) and (C), statistical significance was calculated using a longitudinal mixed-effects model in which si3e and si3d were both compared to siCtrl. Data are represented as the mean ± SEM from 6–9 replicates per time point and condition.

(D) Density and contour plot of the normalized invasive area (x axis) and the GFP:dsRed ratio (*y* axis) for siCtrl (left), si3e (middle), and si3d (right). The Spearman correlation coefficient and *p* value are denoted for each.

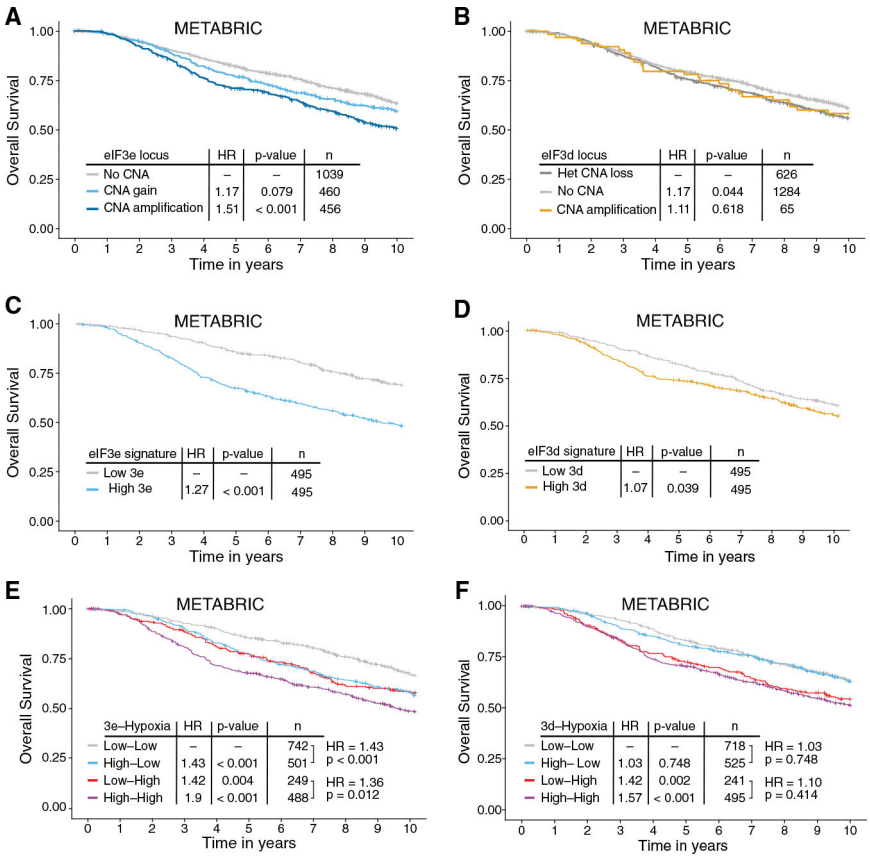

Figure 4. eIF3e-associated RNA signature predicts poor prognosis

(A and B) Overall survival rates of METABRIC patients (n = 1980) with breast tumor (A) eIF3e gains/amplifications or (B) eIF3d gains/amplifications compared to no copy-number alterations (CNAs) in the METABRIC dataset.

(C and D) Overall survival of patients in the METABRIC datasets stratified by (C) eIF3e and (D) eIF3d RNA-seq signatures using the intersection of targets in both MCF7-SIX1 and MDA-MB-231 cells. For clarity, only the first and fourth quartiles are shown.

(E and F) Overall survival rates of patients in the METABRIC dataset stratified by (E) the combination of hypoxia signature and eIF3e or (F) eIF3d enrichment/depletion. The p values and hazard ratios were calculated using a Cox proportional hazards regression where each group was compared to the control group (e.g., no CNAs for eIF3e, heterozygous (het) CNA loss for eIF3d, and bottom 25% for signatures).

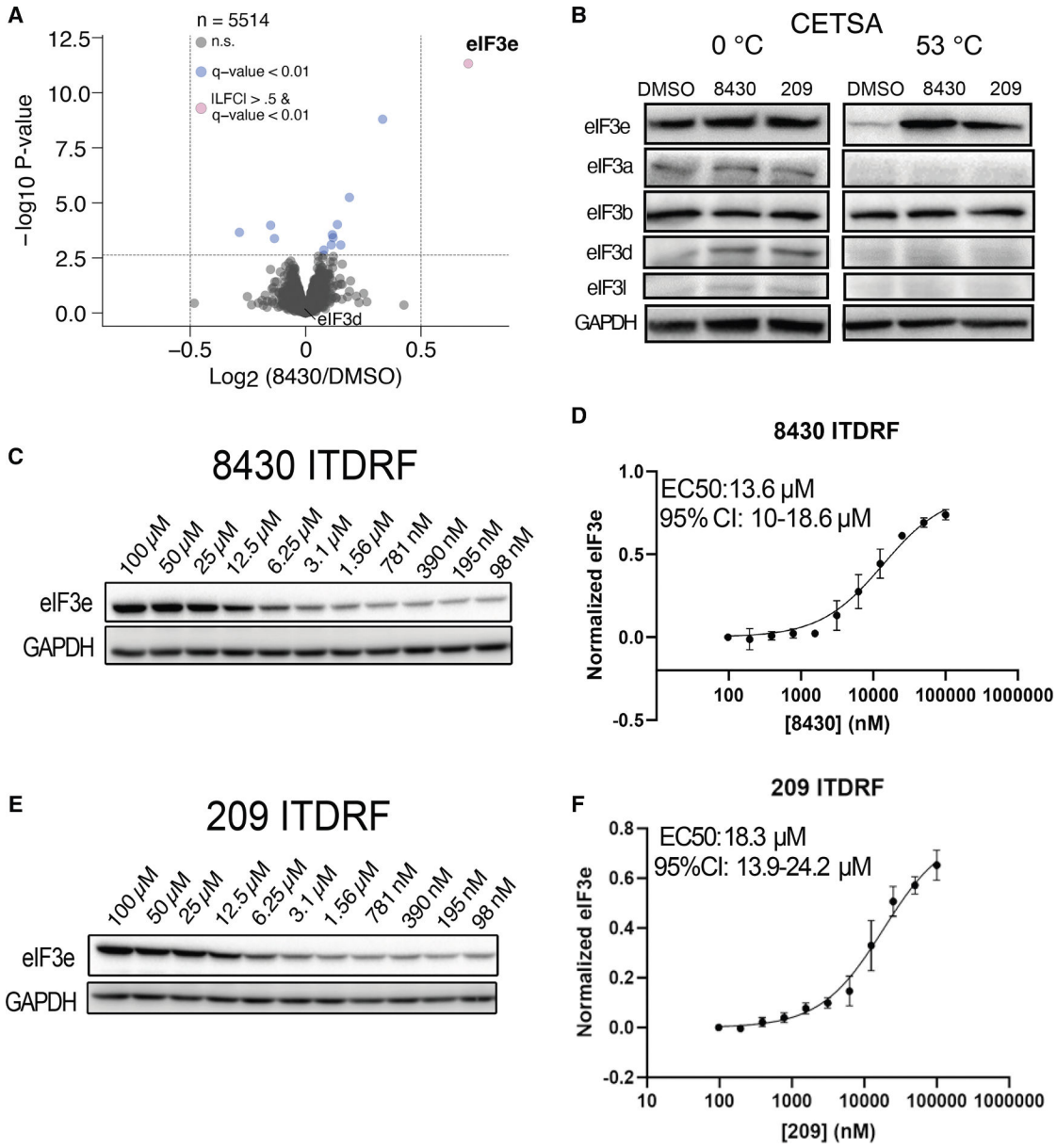

Figure 5. Compounds 8430 and 209 specifically stabilize eIF3e protein in thermal shift assays

(A) Volcano plot of the isothermal shift assay (ITSA) with log2 fold change (*x* axis) and −log10 *p* value (*y* axis).

(B) Cellular thermal shift assay (CETSA) followed by western blot showing protein levels of eIF3e and multiple other eIF3 subunits in addition to the loading control of GAPDH.

(C and D) Dose response of 8430 for an isothermal dose-response fingerprint (ITDRF) assay.

(E and F) Dose response of 209 for an ITDRF assay.

For (D) and (F), data are represented as the mean ± SD from 3 replicates.

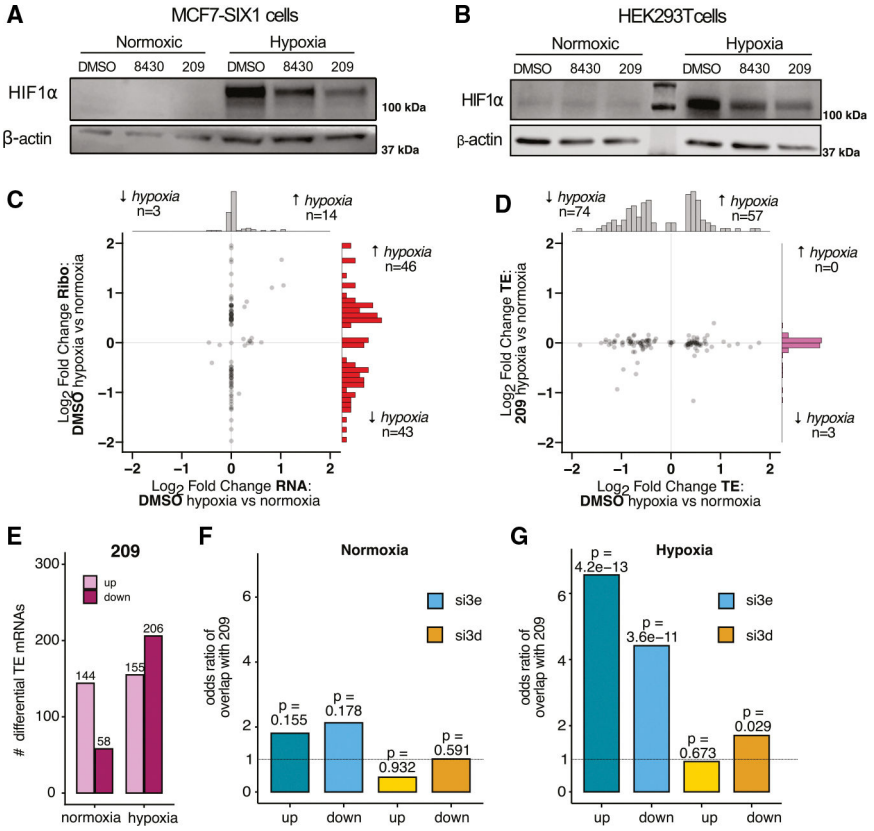

Figure 6. Small-molecule compounds, 8430 and 209, inhibit the acute translational hypoxic response

(A and B) Western blot analysis showing HIF1α after 8430 and 209 treatment (24 h pre-treatment) in normoxic and hypoxic (4 h at 1%O2) conditions for (A) MCF7-SIX1 and (B) HEK293T cells.

(C) Log_2 fold change of RPFs (*y* axis) and RNA levels (*x* axis) comparing DMSO treatment in normoxia vs. hypoxia in MCF7-SIX1 cells. Each dot represents a mRNA transcript.

(D) Comparison of significant TE changes from normoxia to hypoxia in DMSO-treated cells (*x* axis) to TE changes from normoxia to hypoxia after treatment with a209 (*y* axis).

(E) Barplot of the number of differentially translated mRNAs with 209 treatment in normoxia and hypoxia.

(F and G) Barplot of the odds ratio for the overlap of mRNA with TE changes in a209 treatment compared to those with TE changes in eIF3e or eIF3d KD in (F) normoxia and (G) hypoxia. *p* values were calculated using Fisher's exact test.

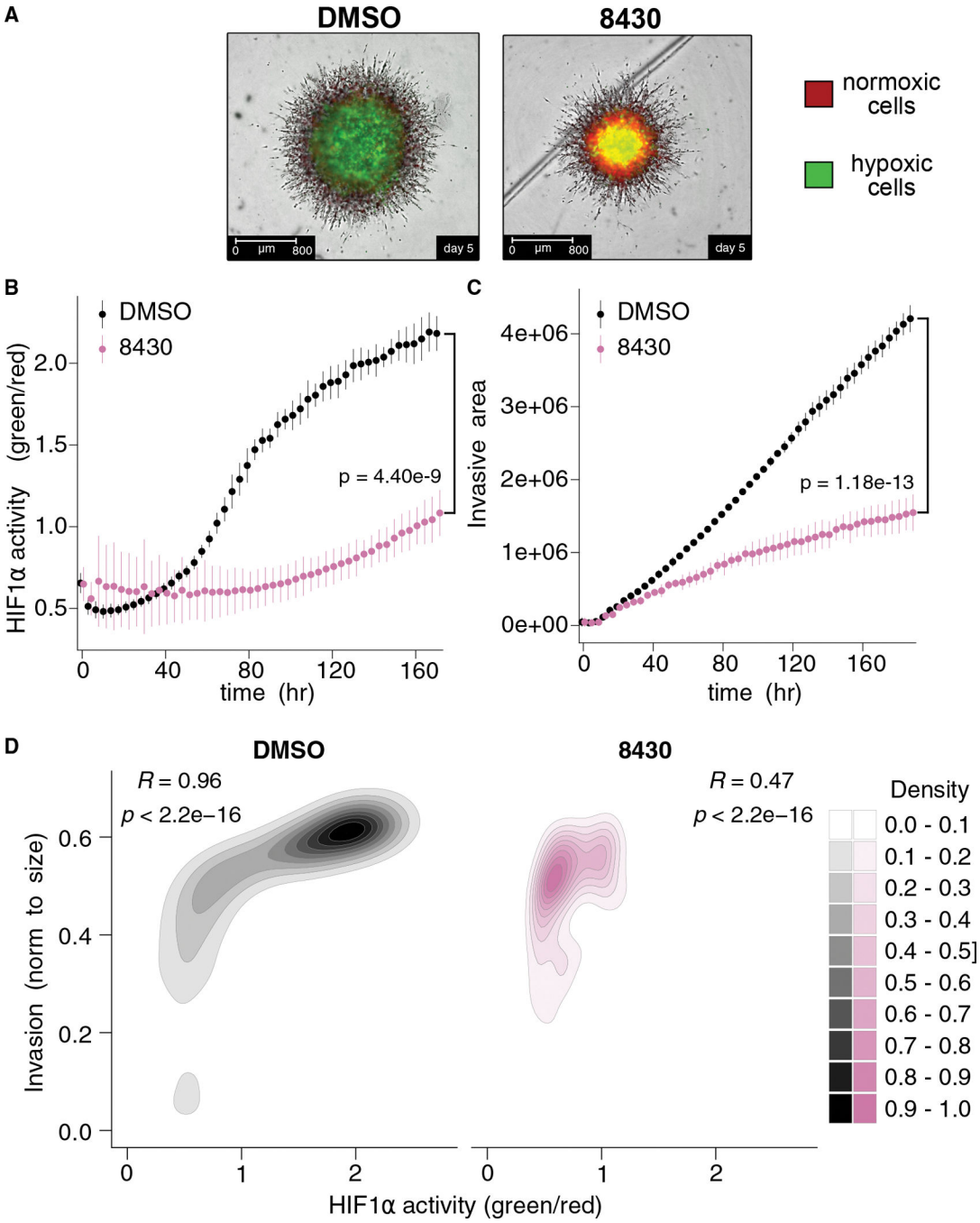

Figure 7. 8430 inhibits HIF1α-mediated effects and tumorsphere invasion

(A) Representative images of 231HFM cells grown in tumorspheres embedded in Matrigel and collagen I ± 8430 treatment.

(B) Fluorescence ratio of GFP:dsRed over time ± 8430 treatment.

(C) Invasive area of the 231 tumorspheres over time ± 8430 treatment.

For (B) and (C), statistical significance was calculated using a longitudinal mixed-effects model comparing 209 to DMSO. Data are represented as the mean ± SEM from 6–9 replicates per time point and condition.

(D) Density and contour plot comparing the normalized invasive area (*y* axis) and the GFP:dsRed ratio (*x* axis) in DMSO (left) and 8430 (right) treatment. The Spearman correlation coefficient and *p* value are denoted for each.

KEY RESOURCES TABLE

REAGENT or RESOURCE	SOURCE	IDENTIFIER
Antibodies		
RABBIT ANTI-EIF3A	Bethyl	*Cat# A302-002A, RRID:AB_1576520)*
RABBIT ANTI-EIF3B	Bethyl	*Cat# A301-761A; RRID: AB_1210995*
RABBIT ANTI-EIF3D/EIF3S7	Bethyl	*Cat# A301-758A; RRID: AB_1210970*
RABBIT ANTI-EIF3E	Abcam	*Cat# ab36766, RRID:AB_869604*
Rabbit anti-EIF3L	Bethyl	Cat# A304-753A, RRID:AB_2620948)
Rabbit anti-RB1CC1	Proteintech	Cat# 17250-1-AP, RRID:AB_10666428)
Rabbit anti-PCBP2	Thermo Fisher Scientific	Cat# PA5-30116, RRID:AB_2547590)
Rabbit anti-Pan TEAD	Cell Signaling Technology	Cat# 13295, RRID:AB_2687902
Rabbit anti-vinculin	Cell Signaling Technology	Cat# 13901, RRID:AB_2728768
Mouse anti-beta-actin	Sigma-Aldrich	Cat# A5316, RRID:AB_476743
Goat anti-Rabbit HRP	Licor	*Cat#: 926–80011 RRID AB_2721264*
Goat anti-Mouse HRP	Licor	Cat#: 926–80010: RRID AB_2721263
Rabbit polyclonal anti-GAPDH	Cell Signaling Technology	Cat#: 5174S, RRID:AB_10622025
Chemicals, peptides, and recombinant proteins		
Opti-MEM I Reduced Serum Medium	ThermoFisher Scientific	Cat# **31985062**
Lipofectamine RNAIMAX Transfection reagent	Thermo Fisher Scientific	Cat#: 13778150
Phosphate-Buffered Saline pH7.4	ThermoFisher Scientific	Cat# AM9625
Bovine-Serum Albumin	Bioworld	Cat# 22070008-1
Ampicillin	Sigma-Aldrich	A9518
DMSO	ThermoFisher Scientific	Cat# BP231100
SuperSignal West Pico PLUS	ThermoFisher Scientific	Cat# 34579
Thermo Scientific Restore Plus Western Blot Stripping Buffer	ThermoFisher Scientific	Cat# 46430
SUPERaseIN	ThermoFisher Scientific	Cat# AM2694
750 U RNase I	Invitrogen Ambion	Cat# AM2294
Trizol LS Reagent	ThermoFisher Scientific	Cat# 10296028
Igepal® CA-630	Sigma-Aldrich	Cat# I8896
cOmplete™ Mini EDTA-free Protease Inhibitor Cocktail	Sigma-Aldrich	Cat# 11836170001
Pierce™ Phosphatase Inhibitor Mini Tablets	Thermo Fisher Scientific	Cat# A32957
BCA Protein Assay Kit	Thermo Fisher Scientific	Cat# 23225
4titude Random Access PCR Plate, 96-well, sealable	Azenta	Cat# 4ti-0960/RA
Guanidine Hydrochloride	Sigma-Aldrich	Cat# G3272
HEPES (≥99.5% titration grade)	Sigma-Aldrich	Cat# H3375
Tris(2-carboxyethyl)phosphine (TCEP)	Thermo Fisher Scientific	Cat# 20490
2-Chloroacetamide	Sigma-Aldrich	Cat# C0267
Lysyl Endopeptidase (Lys-C)	Wako (FUJIFILM)	Cat# 129-02541
Sequencing Grade Modified Trypsin	Sigma-Aldrich	Cat# T6567
TMT10plex™ Isobaric Label Reagent Set	Thermo Fisher Scientific	Cat# 90110

REAGENT or RESOURCE	SOURCE	IDENTIFIER
DMSO (≥99.9%, cell culture grade)	Sigma-Aldrich	Cat# D8418
Critical commercial assays		
ZYMO Directzol RNA microprep kit	ZYMO Research	Cat# R2062
KAPA RNA Hyper prep RNAseq l ibrary prep kit	Roche	Cat# 08098107702
KAPA Unique Dual-Indexed Adapter Kit	Roche	Cat# 08861919702
Tapestation High Sensitivity D1000 ScreenTape	Agilent	Cat# 5067-5585
Qubit dsDNA HS assay	ThermoFisher Scientific	Cat# Q32851
Qubit RNA BR assay kit	ThermoFisher Scientific	Cat# Q10210
Human Ribo-Seq rRNA Depletion kit	siTOOLs Biotech	Cat# dp-K096-042
QIAseq miRNA library prep kit	Qiagen	Cat# 331502
QIAseq miRNA 96 Index IL (96)	Qiagen	Cat# 331565
Illustra Microspin S-400 HR columns	VWR	Cat# 27-5140-01
MycoAlert Detection kit	Lonza	LT07-418
Deposited data		
RNA-Seq	This paper	GSE307666
Ribo-Seq	This paper	GSE307666
Experimental models: Cell lines		
Human: MCF7-SIX1	Ford et al.[47]	N/A
Human: MDA-MB-231 (parentals)	University of Colorado Cell Technologies Shared Resource	RRID:CVCL_0062 RRID: SCR_021982
Human: MDA-MB-231 hypoxia fate-mapping (231HFM)	Godet et al.[57]	N/A
Human: HEK293T	University of Colorado Cell Technologies Shared Resource	RRID:CVCL_0063 RRID: SCR_021982
Oligonucleotides		
ON-TARGETplus Human EIF3E siRNA SMART POOL	Horizon Discovery	L-010518-00-0005
ON-TARGETplus Human EIF3D siRNA SMART POOL	Horizon Discovery	L-017556-00-0005
siGENOME Non-Targeting siRNA Control Pool	Horizon Discovery	D-001810-10-05
Original code		
Ribosome profiling analysis pipeline	This paper	Github link
Recombinant DNA		
Plasmid: Bidirectional Luciferase backbone	Mukherjee Lab	N/A
Software and algorithms		
R version 4.1.6	CRAN	https://www.r-project.org/
R studio	posit	https://www.rstudio.com/
ImageJ	ImageJ	https://imagej.net/ij/

REAGENT or RESOURCE	SOURCE	IDENTIFIER
Tidyverse	Wickham et al.[80]	https://www.tidyverse.org/
Tximport	Soneson et al.[79]	https://bioconductor.org/packages/release/bioc/html/tximport.html
ggplot2	Wickham et al.[80]	https://ggplot2.tidyverse.org/
DESeq2	Love et al.[81]	https://bioconductor.org/packages/release/bioc/html/DESeq2.html
Bowtie2	Langmead et al.[82]	https://bowtie-bio.sourceforge.net/bowtie2
Cutadapt	Martin[83]	https://pypi.org/project/cutadapt/
SAMtools	Li et al.[41]	http://www.htslib.org
STAR	Dobin et al.	https://github.com/alexdobin/STAR
UMItools	Smith et al.[84]	https://github.com/CGATOxford/UMI-tools
Salmonv1.6	Patro et al.[85]	https://salmon.readthedocs.io/en/latest/salmon.html
Enhanced Volcano	Blighe et al.[86]	https://bioconductor.org/packages/release/bioc/html/EnhancedVolcano.html
rstatix	Kassambara et al.[87]	https://rpkgs.datanovia.com/rstatix/
MaxQuant	Max Planck Institute/Cox Lab	Version 1.6.3.3 (www.maxquant.org)
Perseus	Max Planck Institute/Cox Lab	Version 1.6.1.3
limma (R Bioconductor package)	Bioconductor	Version 3.38.3
Instruments		
Orbitrap Fusion Tribrid Mass Spectrometer	Thermo Fisher Scientific	Model: Orbitrap Fusion
Waters M-class Acquity UPLC	Waters Corporation	Model: Acquity M-class
Agilent 1100 HPLC System	Agilent Technologies	Model: 1100 Series
Eppendorf ThermoMixer C	Eppendorf	Cat# 5382000015
Bioruptor Sonicator	Diagenode	Model: Bioruptor UCD-200